UNIVERSITY OF CAMBRIDGE

DEPARTMENT OF MATERIALS SCIENCE AND METALLURGY

Electromagnetic Modelling of Superconducting Sensor Designs

Guido Gerra

Clare Hall, University of Cambridge

Preface

The present dissertation has been submitted for the degree of *Master of Philosophy* in Materials Modelling at the University of Cambridge, for the academic year 2002-2003. The research described herein was conducted under the supervision of Dr. Edward Tarte within the Device Materials Group in the Department of Materials Science and Metallurgy, University of Cambridge, between May and August 2003.

Except where acknowledgement and reference are made to previous work, the information contained in this dissertation is the result of my own work. The sources of information of which I have availed myself are clearly referenced throughout the text and are listed in detail in the bibliography at the end of the report.

I hereby declare that my thesis is not substantially the same as any that I have submitted for a degree or diploma or other qualification at any other University. I further state that no part of my thesis has already been or is being concurrently submitted for any such degree, diploma or other qualification.

The length of this thesis does not exceed the prescribed limit of 15,000 words.

Guido Gerra

Cambridge, August 2003

Contents

Acknowledgements

I would like to thank my supervisor, Dr. Edward Tarte, for all his support and assistance and the competent and stimulating guidance he has provided me with during the project.

I am very much indebted to the academic staff that was involved in the MPhil in Materials Modelling, for making the course such a valuable experience, a special mention going to Dr. Zoe Barber, Prof. Harry Bhadeshia, Dr. James Elliot and Dr. Phil Hasnip.

I would like to thank my girlfriend, Claudia Cancellieri, and my parents, Gaetana Fanelli and Giovanni Gerra, for their continued and invaluable moral support in difficult times. I express personal gratitude to all the other MPhil students – Barry, Ed, Helen, Katerina, Kristin, Mohamed, Yi and Yixuan – and to my tutor, Dr. Armando Genazzani. The staff at Clare Hall also deserves a mention.

Finally, a special thanks to my three housemates – Jorge Arenas-Vidal, Foo Shao Tyng and Panagiotis Nikolopoulos – for their friendship and for all the moments they have shared with me.

Abstract

The problem of design optimisation of thin film direct current Superconducting QUantum Interference Device (SQUID) magnetometers made of YBCO ($YBa_2Cu_3O_{7-x}$) was considered. The inductances and effective areas were calculated using the software package 3D-MLSI. Resolution and reliability issues were first tested on simple superconducting systems, showing good agreement with analytical formulae and experimental results, and demonstrating that a remarkable precision can be obtained though at the expense of CPU time and memory. The software was then used to simulate a SQUID magnetometer fabricated in the Device Materials Group of the Department of Materials Science and Metallurgy, proving that 3D-MLSI can be used to predict the parameters of real systems with acceptable accuracy.

1. Introduction

Superconducting QUantum Interference Devices are used in a broad range of applications, from geophysics to the life sciences. They are used to measure very small signals, either directly (by quantifying the magnetic flux that links them) or indirectly (by transforming the signal into a current that is then coupled to the SQUID). The main advantage of a SQUID is the possibility to relate very small changes in the current circulating in it to the magnetic field the SQUID is subjected to. This possibility arises from the dynamics of electromagnetic fields in superconductors combined with the Josephson effect, and appropriate coupling schemes can be used to measure quantities that are not necessarily electromagnetic in nature [1].

Because its purpose is the measurement of very small magnetic fields, the sensitivity of a SQUID is the key factor in the fabrication process. Much work has been devoted to the understanding of the operational characteristics of SQUIDs and to the development of these devices. The motivation for this project was the application of computational techniques to the design optimisation of SQUIDs, a task that involves significant effort in terms of time and costs if carried out experimentally. Using the finite element computer program 3D-MLSI, developed by Dr. Mikhail Khapaev of Moscow State University, simulations were performed on simple systems, in order to identify the salient characteristics of superconducting devices and, by comparing the results with experimental data, to test the limits and accuracy of the software. The knowledge thus gained was used to simulate SQUID magnetometers that have actually been produced in the lab.

This report describes the background and outcome of the project in detail. In Chapter 2, an overview of the theory behind SQUID sensors is presented, with a brief digression on the subject of superconductivity and the Josephson effect, and an outline of some of the most common SQUID designs. Chapter 3 is dedicated to the computational method that has been employed in the simulations, along with the mathematical formalism adopted and the analytical formulae that have been used to verify the validity of 3D-MLSI. In Chapter 4, all the results of the simulations are presented and analysed to determine the precision and range of applicability of the program.

2. Theoretical Background

2.1 Superconductivity

Superconductivity is a macroscopic manifestation of a quantum mechanical phenomenon [2]-[5]. It arises from the fact that for some metals at very low temperatures, the electrons near the Fermi surface form bound pairs, known as *Cooper pairs*, which propagate in an electromagnetic field without any resistive loss. The attractive interaction between the electrons is stronger than the Coulomb repulsion. As the temperature increases the number of superconducting pairs decreases, until at a critical temperature T_c (the *transition temperature*) the superconductive property of the metal disappears, and the metal behaves as a normal resistive material.

Another basic feature of superconductors is the *Meissner effect*: magnetic flux cannot penetrate a metal in its superconductive state apart from a very small region near the surface, where all the induced current is concentrated. If a magnetic field is applied and then the temperature decreased below T_c, flux is expelled from the bulk; if the superconductor is in the form of a ring, after removal of the external magnetic field some of the flux inside the hole of the ring is trapped in multiples of a fundamental flux unit, the *flux quantum*.

The Meissner effect is destroyed when the applied magnetic field exceeds a critical value, B_c. The response of a superconductor to this phenomenon places it into one of two categories: type I superconductors show a transition from the superconducting to the normal state at B_c. For type II superconductors, there are a lower and an upper critical field, B_{c1} and B_{c2}. In the intermediate domain, known as the *mixed state*, the superconductor has zero resistance, but quantised flux lines are allowed to enter some regions of the material. At B_{c2} there is a transition to the normal state.

Although the absence of electrical resistance was first observed in 1911 and the exclusion of magnetic flux from a superconductor in 1932, it wasn't until 1957 that a satisfactory microscopic theory was achieved to explain the discoveries. This theory, the Bardeen-Cooper-Schrieffer (BCS) theory, is based on the idea that superconductivity involves an underlying ordering of electrons that overcomes their Coulomb repulsion and thermal disorder. The ordering is created when electrons organise themselves in pairs with antisymmetric spin states (i.e. the total pair spin is zero), because this lowers the energy of the Fermi gas [5]. The pairs of electrons form bosons, which statistically prefer to be in the same state, with the same energy and the same momentum. We therefore have a situation in which a large number of electrons can be described by a common wavefunction $\boldsymbol{\Psi}(\mathbf{r})$

with a specified momentum $\mathbf{p}_s = m\mathbf{v}_s$. In other words, the Cooper pairs take part in a collective motion with velocity $\mathbf{v}_s$, forming a charged *superfluid* that generates a current density $\mathbf{J}_s$:

$$\mathbf{J}_s = -n_s e \mathbf{v}_s \tag{2.1}$$

where n_s is the number density of superconducting electrons, and e is the electronic charge [3].

The fact that the system of superconducting electrons can be described by a collective wavefunction $\Psi(\mathbf{r})$ means that we can write the Schrödinger equation for the superfluid and get all the electrodynamics of a superconductor from this simple description [2]. The result of this quantum mechanical treatment is three equations, which contain all the information we need about currents and fields in a superconductor. The first equation relates the current density to the vector potential $\mathbf{A}$ and the phase θ of the superfluid wavefunction:

$$\Lambda \mathbf{J}_s + \mathbf{A} = -\frac{\hbar}{2e}\vec{\nabla}\theta \tag{2.2}$$

where $\Lambda \equiv \frac{m_e}{n_s e^2}$ is the *London parameter*. The two other equations can be derived directly from equation (2.2), using vector identities and Maxwell's equations [3]. First we have:

$$\Lambda \frac{\partial \mathbf{J}_s}{\partial t} = \mathbf{E} \tag{2.3}$$

This is known as the *first London equation*. It is an acceleration equation describing the motion of superconducting electrons in an external electric field. If a short pulse of electric field is applied, a supercurrent is set up and the superfluid will flow without decay indefinitely. This is the property of zero electrical resistance. For stationary currents, no electric field exists at any point in the superconductor. From equation (2.2), it follows that it is the magnetic field that determines the current flowing in the superconductor, unlike normal conductors where $\mathbf{J} = \sigma\mathbf{E}$. The electric field only determines the time derivative of the current [4]. The last of the three fundamental equations describing superconductivity is:

$$\vec{\nabla} \times (\Lambda \mathbf{J}_s) = -\mathbf{B} \tag{2.4}$$

Equation (2.4) is known as the *second London equation*. From Ampère's law for a static electric field ($\vec{\nabla}\times\mathbf{B}=\mu_0\mathbf{J}$), this result can be written as:

$$\nabla^2\mathbf{B}=\frac{1}{\lambda_L{}^2}\mathbf{B} \tag{2.5}$$

where $\lambda_L \equiv (\Lambda/\mu_0)^{1/2}$ is the *London penetration depth*. Equation (2.5) tells us that each component of the magnetic field **B** decays exponentially from its value at the surface. This is the Meissner effect: the magnetic field can only penetrate the bulk of a superconductor a very short distance, of the order of λ_L, which depends on the material and is usually in the nanometer range. In this narrow region at the boundary of the superconductor flows all the induced current that is required to expel the external field from the bulk. The penetration depth has a temperature dependence of the form [4]:

$$\lambda_L(T)=\lambda_L(0)\left[1-(T/T_c)^4\right]^{-1/2} \tag{2.6}$$

where $\lambda_L(0)$ is the penetration depth at absolute zero (a property of the material) and T_c is the transition temperature.

In introducing the vector potential **A** and the phase θ of the superfluid wavefunction in equation (2.2), we have passed over a rather formal but important point [3]. **A** and θ are quantities that cannot be measured, and are only defined in terms of their derivatives (e.g. $\mathbf{B}=\vec{\nabla}\times\mathbf{A}$), which are related to observable quantities. So if we make the transformation (called a *gauge transformation*):

$$\mathbf{A}' \rightarrow \mathbf{A}+\vec{\nabla}\chi \tag{2.7}$$

$$\theta' \rightarrow \theta-\frac{2e}{\hbar}\chi, \tag{2.8}$$

the observable physical variables (the magnetic field **B** and the current density $\mathbf{J}_s$) remain unchanged, and they are said to be *gauge invariant* (we can see this by substituting $\mathbf{A}'$ and θ' into equation (2.2), and by remembering that the curl of a gradient is always zero). This means that we can select the definition of **A** and θ arbitrarily (by choosing the appropriate value of χ, which must

be a single-valued and differentiable scalar function of space and time) without any loss of physical meaning or validity.

In the theory of superconductivity the gauge takes on a significant role, as it becomes apparent by looking at equation (2.2). By setting the appropriate definition of the gauge, we can simplify the mathematics of a particular problem considerably. For example, if our superconductor is simply connected, the superfluid wavefunction is single-valued and it is convenient to choose χ so that the phase θ is zero everywhere (this is known as the *rigid* gauge, or *London* gauge if the additional condition $\vec{\nabla} \cdot \mathbf{A} = 0$ is assumed). It follows from equation (2.2) that:

$$\Lambda \mathbf{J}_s = -\mathbf{A} \tag{2.9}$$

and that outside the superconductor (where the supercurrent density vanishes):

$$\nabla^2 \mathbf{A} = 0 \tag{2.10}$$

Also, from (2.9) and Ampère's law ($\vec{\nabla} \times \mathbf{B} = \mu_0 \mathbf{J}$), it is straightforward to show that inside the superconductor:

$$\nabla^2 \mathbf{A} = \mathbf{A} / \lambda_L^{\,2} \tag{2.11}$$

The last two equations (the Laplace and Poisson equation respectively), subject to appropriate boundary conditions and the London equations, can be solved numerically or in some cases even analytically to obtain the current and field distribution in a superconductor.

2.2 The Josephson effect

A Josephson junction consists of two superconductors separated by a thin barrier (in the form of an insulator, a normal metal, or a grain boundary) and connected to a circuit. Quantum tunnelling of Cooper pairs through the barrier generates a current I whose magnitude depends on the phase difference of the two wavefunctions across the junction. The analytical solution of the coupled Schrödinger equations yields [2],[4]:

$$I = I_c \sin\phi \tag{2.12}$$

ϕ being the phase difference across the junction. So the supercurrent through the barrier has a maximum value, I_c, known as the *critical current*. A voltage appears across the junction when a supercurrent $I > I_c$ is applied to the circuit; then the phase difference evolves in time linearly with voltage:

$$\frac{\partial\phi}{\partial t} = \frac{2e}{\hbar}V \tag{2.13}$$

The voltage readout reveals information on the current and magnetic field across the junction [4]. For zero applied voltage, a constant dc current flows in the circuit whose maximum value I_c depends on the properties of the junction, on temperature, and on the applied magnetic field. For a non-zero applied dc voltage, $\sin\phi$ oscillates very rapidly ($2e/\hbar \sim 10^{15}\,HzV^{-1}$) and the net supercurrent averaged over a cycle is zero. Note that the rigid gauge introduced in section 2.1 cannot be used in the presence of a junction, as it would require the phase to be zero everywhere and thus the phase difference ϕ to vanish, contrary to our predictions and to physical evidence.

In the presence of an external magnetic field, the phase difference ϕ is changed. This can be seen from equation (2.2), taking a line integral of both sides normal to the junction and far from the surfaces (so that the current density is close to zero). This extra phase difference term,

$$\delta\phi = \int_d \vec{\nabla}\phi \cdot d\mathbf{s} = \frac{2e}{\hbar}\int_d \mathbf{A} \cdot d\mathbf{s} \tag{2.14}$$

is responsible for the modification of the current I in equation (2.12).

Now, if two Josephson junctions are connected in parallel, a supercurrent driven through the circuit experiences interference – like a wave diffracting through a double slit. This is because the phase changes differently (in general) according to the path chosen, and when the currents add up again they are out of phase. For example, in a circuit threaded by a magnetic flux Φ, two identical junctions give rise to a phase difference:

$$\Delta\phi = \frac{2e}{\hbar} \oint_{loop \cdot \Gamma} \mathbf{A} \cdot d\mathbf{s} = \frac{2e}{\hbar}\Phi = 2\pi\Phi/\Phi_0 \tag{2.15}$$

$\Phi_0 \equiv h/2e$ is the *flux quantum*. So the interference pattern has peaks when the flux is a whole number of flux quanta; then $\Delta\phi = 2n\pi$ and constructive interference occurs. We have seen that if we drive a bias current greater than the junctions' critical current through the circuit, a voltage will appear. The external flux will modulate the voltage in a measurable fashion; hence the flux itself can be measured [4].

Note that magnetic flux is not excluded from the hole in the loop (i.e. the parallel circuit) because the latter is not a single superconductor. The two tunnelling barriers attenuate the supercurrents, which cannot act as screening currents in those regions and allow flux to penetrate. Hence the Meissner effect does not apply in this case.

In our treatment of the Josephson effect, we have omitted displacement currents (due to the surface charge densities building up on both interfaces of the barrier) and currents due to the conduction of normal electrons. A way to correct this imprecision is to represent the displacement current as a capacitance, and the conduction of normal electrons as a shunt resistance, both in parallel with the Josephson junction [4]. With these corrections for the tunnelling current the results obtained above still hold.

2.3 The SQUID

A SQUID consists of two Josephson junctions connected in parallel in a superconducting loop of small inductance *L*, as shown in **Figure 2.1** below. A circuit is connected to the device to drive the bias current and measure the voltage. Its use as a sensor of signals (as imperceptible as those of the brain and the heart) requires dimensions in the micron range. The best performance is obtained by low-transition-temperature SQUIDs; nevertheless, these have to operate at liquid helium temperatures (below 4.2 K), difficult and expensive to achieve and maintain. So with the discovery of high-transition-temperature superconductors in 1986, new relatively cheap technical solutions were made available. Thin superconducting films with a high crystalline quality and a thickness of the same order as the London penetration depth (~10-100 nanometers) are the scheme of choice for high-T_c SQUIDs. The compound most often used as a thin film superconductor is YBCO ($YBa_2Cu_3O_{7-x}$), which has a transition temperature above 90K and therefore behaves as a superconductor at liquid nitrogen temperatures (77K). The Josephson junctions in thin film designs are usually bicrystal grain boundaries: the film is produced by epitaxial growth on a bicrystal substrate with a misorientation angle θ [1].

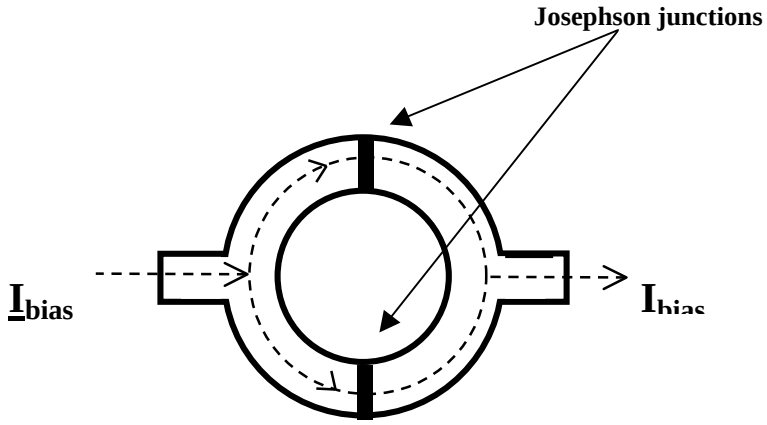

Figure 2.1: Simplified diagram of a SQUID.

We have mentioned above that a Josephson junction can be seen as a resistively and capacitively shunted junction. When two such junctions are connected in parallel, hysteresis (i.e. irreversibility of the I-V characteristics of the circuit) can become a problem. This is avoided if the McCumber condition,

$$\beta_c \equiv 2\pi I_0 R^2 C / \Phi_0 \lesssim 1 \qquad (2.16)$$

is satisfied (here, I_0 is the Josephson critical current, R the resistance and C the capacitance of the junctions) [1].

When dealing with very small signals, flux noise deeply affects the sensitivity of the sensor. The Nyquist noise currents in the shunt resistors produce white voltage and current noise in the SQUID. This effect poses a constraint on the system parameters, in that the magnetic energy per flux quantum stored in the SQUID must be much greater than the noise energy (i.e. $\Phi_0^2/2L \gg 2\pi k_B T$). Moreover, an important condition for optimisation is that [1]:

$$\beta_L \equiv \frac{2LI_0}{\Phi_0} \approx 1 \tag{2.17}$$

In view of all these considerations on the SQUID parameters and the experimental data available, the optimal SQUID inductance L is found to lie in a range of a few tens of pH [1],[6]-[9]. L is a key parameter in the design of efficient sensors.

Another source of flux noise is the motion of flux vortices in the SQUID loop. Because YBCO is a type II superconductor, when it is cooled down to its superconducting state in the presence of a magnetic field higher than its first critical field B_{c1}, which is typically very low, magnetic flux is not excluded from the bulk: flux vortices (*fluxons*) can be observed, confined in certain regions within a matrix of flux-excluding material. (This effect is particularly evident when the superconductor is cooled in the earth's magnetic field.) The effect of finite temperature is to thermally activate the hopping of flux vortices between pinning sites (the nature of which is still unknown) in the superconducting film. This generates low frequency flux noise. For high-T_c superconductors such as YBCO, usually operating at liquid N_2 temperatures, thermal energies, and thus flux hopping, cannot be neglected. Making the linewidths of the films narrow enough reduces this noise because it is energetically unfavourable for vortices to enter. Improving the crystalline quality also reduces flux hopping, but on the other hand it decreases the density of pinning sites, which are crucial to maintain flux vortices under control. Because the phenomenon is not yet fully understood, there is no quantitative description of the dependence of low frequency flux-noise on flux hopping; therefore direct noise measurements are required to determine the quality of a film [1],[3].

A SQUID is very sensitive to changes in magnetic flux, but because of its small area its sensitivity to changes in magnetic field is low. The magnetic-field noise at a given frequency is $S_B^{1/2}(f) = S_\Phi^{1/2}(f)/A_{eff}$ [7]. Consequently, the SQUID is often coupled to a flux transformer to

increase the effective area A_{eff} of the device without enhancing the flux noise $S_\Phi(f)$. Alternatively, a square washer design can be adopted, where flux is focussed into a hole representing the SQUID loop. The SQUID-flux transformer system is known as a magnetometer, of which there exist two classes: directly coupled and multiturn flux-transformer magnetometers. Here we are interested mainly in the first type.

2.3.1 Square washers

A square washer is a square superconducting film of length *D* and with an inner hole of length *d* (see **Figure 2.2** below). The wide inductive square loop of the SQUID acts as the single turn coil of a flux transformer [10]. Flux is expelled from the film and is partly focussed into the inner hole. A screening supercurrent is induced along the outer and inner perimeters of the washer (with a fast-decaying tail moving away from the edges). Moreover, a bias current greater than the junctions' critical current is applied in order to measure the voltage across the circuit. (The bias current has no inductive effect because it does not circulate in a loop.) If we neglect the inductance of the slit, computer simulations show that the inductance of the SQUID approaches a constant value, $L = 1.25\mu_0 d$, when the width $W = (D-d)/2$ of the loop becomes of the order of or greater than the width of the hole, *d* [10].

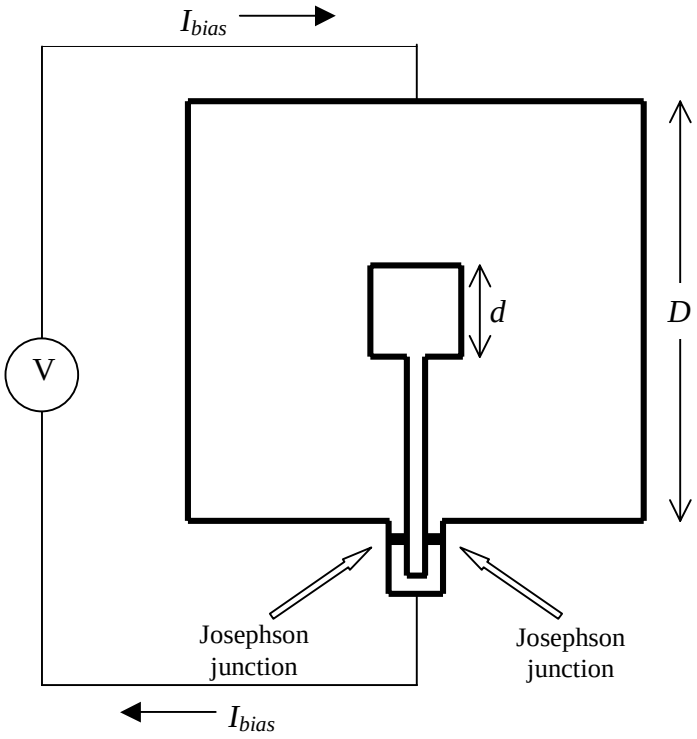

Figure 2.2: Schematic representation of a square washer SQUID design.

Also, in analogy with the case of a circular washer of the same width, the effective area can be found analytically to be $A_{eff} \approx dD$ [6]. Now, if the Josephson junctions are close enough to the hole, the flux that they see is approximately that through the hole. If, on the other hand, they are near the outer edge of the washer, the slit inductance can become important because it is proportional to the length $l \approx W$ of the slit: $L_{slit} \approx (0.3 - 0.4 l/\mu m) pH$ [1]. The effective area though is significantly increased as the slit length increases. So if we want to maximise the effective area without increasing the inductance beyond a few tens of pH, we need to find a compromise, which limits the washer size to a few hundreds of microns. This is a task where computer simulations can play an invaluable part, as preparing SQUIDs of different shapes and sizes just for optimisation purposes is costly.

Although the SQUID inductance can be calculated by summing the hole inductance ($L_h = 1.25 \mu_0 d$) to the slit inductance ($L_{slit} \approx (0.3 - 0.4 l/\mu m) pH$), this method is often too inaccurate for high-sensitivity sensors. The slit inductance includes the contribution of the Josephson junction striplines (the u-shaped strip below the junctions in **Figure 2.2**), although it is highly unfavourable for the screening supercurrent to follow that path. Also, in general, for more complicated shapes the approximations for the inductances given above do not apply. This problem thus requires a numerical treatment, e.g. solving the London equations subject to the appropriate Maxwell's equations for a given geometry [1],[11]-[13].

2.3.2 Directly coupled magnetometers

In directly coupled magnetometers [7], a large pickup loop is patterned in the same layer as the SQUID so that the supercurrent produced by an applied magnetic field is injected directly into the body of the SQUID (see **Figure 2.3** below). These single layer devices are relatively simple to produce, but the flux-coupling efficiency is reduced with respect to multiturn flux-transformers due to a mismatch in the inductances of the pickup loop and the SQUID. Overall, though, they are often preferable over multilayer designs thanks to their lower low-frequency noise and dimensions.

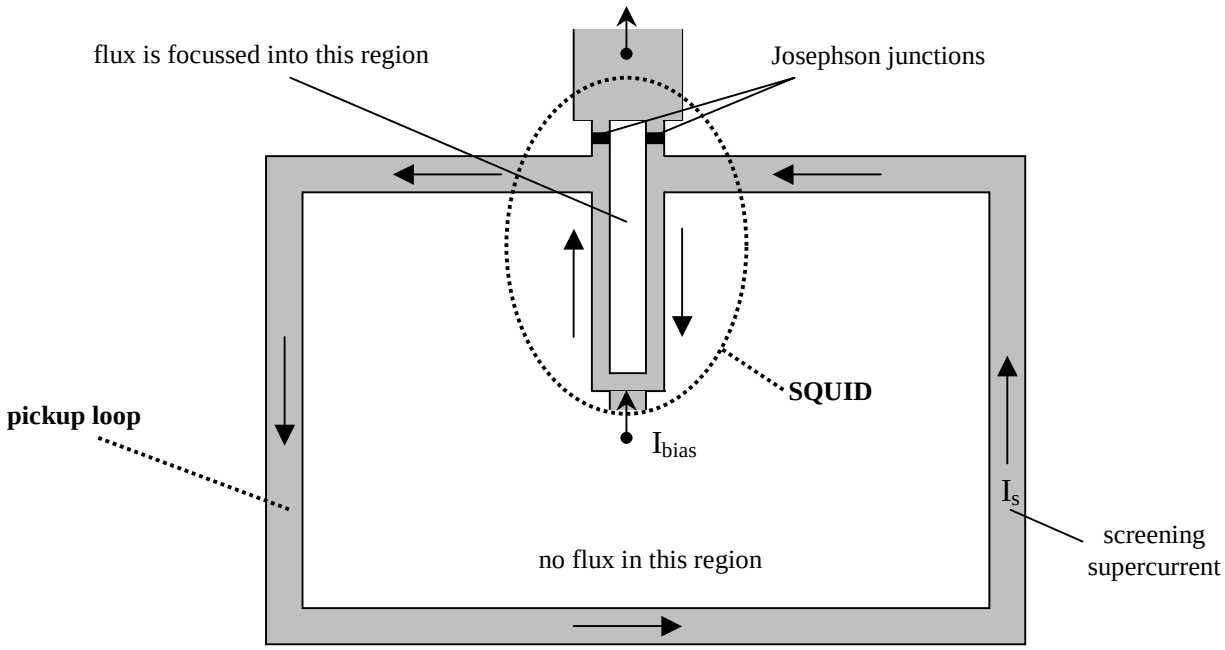

Figure 2.3: Directly coupled magnetometer. The pickup loop is connected directly to the hairpin-shaped SQUID. The screening current enters from the right-hand side and flows around the slit clockwise. The bias current flows vertically.

The idea behind SQUID sensors is to relate a measurable voltage to a magnetic field B. What the voltage tells us is the flux threading the SQUID. This is the sum of the external magnetic flux that enters the SQUID hole directly, plus the fraction of flux that the pickup loop focuses into the SQUID hole. Let A_S, Φ_S, L_S and A_p, Φ_p, L_p be the effective area, the flux, and the inductance of the SQUID and the pickup loop respectively. Let A_{eff} be the effective area of the magnetometer. If we can assume the field B to be uniform over the area occupied by the SQUID, we have:

$$\begin{aligned} BA_{eff} &= \textit{flux threading the SQUID} = \\ &= \textit{external flux} + \textit{flux focused by the pickup loop} = \\ &= BA_S + \Phi_S \end{aligned} \tag{2.18}$$

Now, the same supercurrent I flows both in the pickup loop and in the SQUID. The pickup loop is a closed loop, so it follows from the Meissner effect that this supercurrent I must generate a flux Φ_p, which is equal and opposite to the external flux threading the hole in the pickup loop. The

flux Φ_p produced by the pickup loop to screen the external flux, and the flux Φ_S focused by the pickup loop into the SQUID, have the following relationship:

$$\begin{aligned} \Phi_p &= L_p I \\ \Phi_S &= L_S I = \frac{L_S}{L_p}\Phi_p \end{aligned} \tag{2.19}$$

Substituting (2.19) into (2.18), we obtain a formula for the total effective area:

$$A_{eff} = A_S + \frac{\Phi_S}{B} = \frac{L_S}{L_p}\frac{\Phi_p}{B} + A_S = \frac{L_S}{L_p}A_p + A_S \tag{2.20}$$

So if the effective areas and the inductances are known from numerical methods, the magnetic field *B* ensues. Given a numerical method to evaluate mutual and self-inductances, a reference source can be used to determine effective areas. For example, we can use a short strip length ℓ acting as an electric dipole, with a constant current *I* and mutual inductance with the SQUID (or pickup loop) *M*. *M* is found via the same numerical techniques as for the self-inductances. At large distances ($r \gg \ell$), the strip generates an approximately uniform magnetic field $B(r) = \mu_0 \ell I / 4\pi r^2$ [14]. The flux induced by the strip is $\Phi = MI$. Hence the effective area is:

$$A_{eff} = \lim_{r\to\infty}\frac{\Phi}{B} = \lim_{r\to\infty}\frac{MI}{\left(\mu_0 \ell I / 4\pi r^2\right)} = \lim_{r\to\infty}\frac{4\pi}{\mu_0}\frac{Mr^2}{\ell} \tag{2.21}$$

Because the effective area is an intrinsic property of a magnetometer, we expect the slope of a graph of M vs. $1/r^2$ to tend to a constant limiting value of $\mu_0 \ell A_{eff} / 4\pi$ as $r \to \infty$.

2.3.3 Inductance calculation

We have seen that the problem of calculating the magnetic field *B* given the readout of the flux transformer reduces to the calculation of inductances. One way to do this is numerically [11]-[13],[15]-[17]. The general approach is to consider the energy of a system, solve the appropriate London and Maxwell equations for the specific geometry and penetration depth, and relate the

current distribution to the energy (which is a functional of the current density). This set of equations, satisfied by the vector potential, can be shown to be equivalent to the Laplace equation of electrostatics outside the superconductor and to the Poisson equation inside [18]. This means that with the appropriate boundary conditions we can solve for the current density at a discrete number of points in the superconductor, and using a finite element method compute the total energy of the system. The boundary conditions are $\nabla \cdot \mathbf{A} = 0$ and that the component of **A** normal to the thin film is zero.

The energy of the system has a magnetic term and a kinetic term. The latter originates from the fact that the superconducting electrons move without dissipation, so the energy required to accelerate them is stored in their motion. Because the velocity of the electrons is proportional to the current density *J*, the kinetic energy is proportional to J^2. The magnetic term is proportional to the square of the magnetic field, and via the London equations, Maxwell's equations, and the Biot-Savart law, it can be reduced to a double integral in the current density [11]. The energy functional for a thin superconducting film has the form:

$$E = \frac{\mu_0}{2}\int_V {\lambda_L}^2 \mathbf{J}^2 dv + \frac{\mu_0}{8\pi}\int_V\int_V \frac{\mathbf{J}(\mathbf{r})\cdot\mathbf{J}(\mathbf{r}')}{|\mathbf{r}-\mathbf{r}'|} d\mathbf{r}d\mathbf{r}' \qquad (2.22)$$

where λ_L is the London penetration depth, **J** the current density and the integration is over the entire superconducting region. The contribution of external magnetic fields is included in **J**. If most computational techniques to calculate inductances are based on a total energy evaluation approach, they differ in the way the current distribution is simulated. In [11] and [12], for example, the current density **J** in equation (2.22) was calculated directly by minimizing free energy with a variational technique. These methods proved to have limitations in their applicability and were time and memory consuming [15]. In the present project the problem of inductance calculation was tackled with the use of the computer program 3D-MLSI [16]. The method used in 3D-MLSI to solve for the energy in equation (2.22) is based on the representation of the current density as a scalar potential function, on the solution of appropriate electrostatic equations and boundary conditions, and on the simulation of piecewise-constant currents circulating on a triangular finite element mesh [13]. Evidence will be produced in the course of this report of the accuracy and computer efficiency of this method.

Once the energy of the system is known, it is straightforward to calculate the mutual and self-inductances of its components, which are holes and terminal paths. It will be shown in section 3 that the energy is a quadratic form in the currents circulating around holes and between terminals,

the coefficients of the form being the mutual and self-inductances of the various system components. A simple iterative process can be used to extract the inductances from the total energy, by sequentially assigning arbitrary values (e.g. 1 for a single or pair of components and 0 for all the others) to the currents and calculating the energy at each step.

3. Experimental Method

3.1 The Code: 3D-MLSI

3D-MLSI is a finite element software package developed by Dr. Mikhail Khapaev of Moscow State University [16]. Finite element methods are used in a wide range of engineering applications. The basic concept is to map what is usually a continuous function into a discrete set of values, thus enabling a computer to perform numerical calculations. The object under investigation is divided into a grid of small elements (the *mesh*), and the property that we wish to simulate (such as temperature, stress, or in the present case current density) is defined at each node of the grid. Given some boundary conditions, the list of values at the nodes is calculated by the appropriate computer program at each step in the simulation, giving the overall variation of the required property in space or time.

The first feature in 3D-MLSI's algorithm is the transformation of a three-dimensional picture into a two-dimensional representation of the system of superconductors (see **Figure 3.1** below). For this simplification we require the conductors to have a thickness of the same order as the penetration depth, and the other linear sizes to be much greater (in other words, the method applies to thin films). This enables us to neglect the components of the current and of the field in the direction perpendicular to the film (e.g. the *z*-direction), and to eliminate the *z*-dependence of all the quantities by taking averages over the thickness [13].

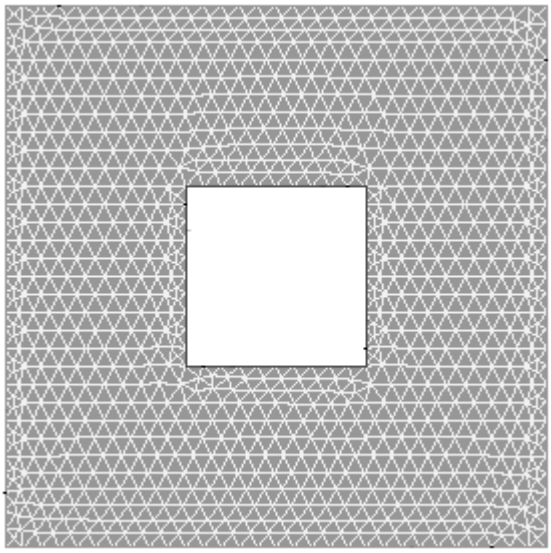

Figure 3.1: example of how the mesh is generated by 3D-MLSI in the case of a square washer with a hole.

The program generates a 2D triangular mesh automatically (according to the shape of the conductors), with a resolution step adjustable by the user. The appropriate electrodynamical equations and boundary conditions are transformed into a system of linear and quadratic equations in a scalar potential, the *stream function*, which is introduced for the purpose of mathematical simplification. The stream function is a potential-function representation of the two-dimensional sheet current flowing on the film, is defined in terms of its derivatives and has the physical meaning of the total current through a component of the circuit [13]. The advantage of this representation is that a complex system with, in general, no analytical solution can be solved numerically: the boundary conditions fix the value of the stream function at the external nodes of the mesh (i.e. the nodes on the edges of the conductors), while everywhere else the value of the stream function is worked out from the electrodynamical equations using a numerical algorithm common to many finite element problems [15],[19]. Because the stream function is related to the current density, the current distribution in the system is a direct output of the numerical solution (see **Figure 3.2**). At the same time, the energy of the system can be shown to be a quadratic form of the stream function, and from the total energy the inductances can be obtained directly [18]. A rigorous derivation of the method employed by 3D-MLSI can be found in [13].

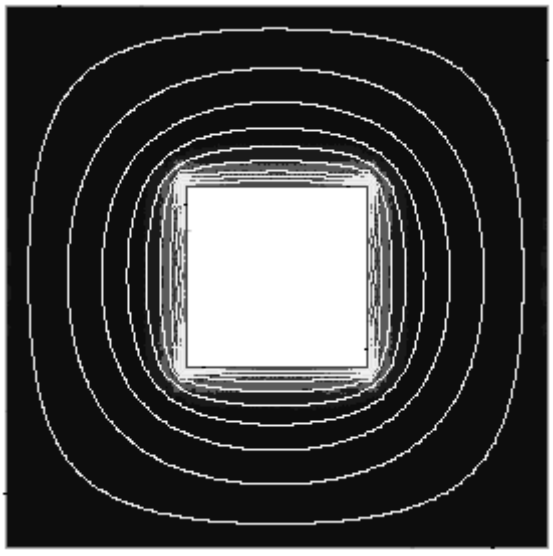

Figure 3.2: current distribution for the square washer of Figure 3.1. The colour scheme describes the current intensity, from dark blue (lowest) to yellow (highest). The white lines represent the current flow paths.

The program 3D-MLSI is divided into three parts: a pre-processor, a numerical core and a tool for the extraction of inductances [20]. The pre-processor is a program that takes an input file

with the specifications of the system of superconductors and generates the triangular mesh. The files with the information about the mesh are then fed to the numerical core, which performs the finite element calculations on the stream function.

Once the numerical core produces its output, the total energy of the system, another algorithm is required to extract the inductance matrix. The total energy of a system consisting of N components is [21]:

$$E = \sum_{i=1}^{N} E_i = \sum_{i=1}^{N} \left[\frac{1}{2} L_i {I_i}^2 + \frac{1}{2} \left(I_i M_{i1} I_1 + I_i M_{i2} I_2 + ... + I_i M_{iN} I_N \right) \right] \tag{3.1}$$

where L_i is the self-inductance of component i, I_i the current circulating through i, and M_{ij} the mutual inductance between components i and j. The expression above can be written more simply in matrix form:

$$E = \frac{1}{2} \mathbf{I}^T L \mathbf{I} \tag{3.2}$$

where $\mathbf{I} = (I_1, ..., I_N)$ is a vector containing all circulating currents and L is called the *inductance matrix*. The diagonal elements of L are the self-inductances of the system, while the off-diagonal terms are the mutual inductances. Note that because $M_{ij} = M_{ji}$ (reciprocity of the mutual inductance), matrix L is *symmetric*.

If we set the boundary conditions so that the current through each component is zero except for component i ($I_j = \delta_{ij}$), calculate the total energy, and then repeat the procedure for all components, we get the self-inductances of the system directly from the energy:

$$L_i = 2E / {I_i}^2 \tag{3.3}$$

If we then set all currents but a pair i, j to zero ($I_l = \delta_{il} + \delta_{jl}$), we obtain the mutual inductances:

$$M_{ij} = \left(2E - L_i {I_i}^2 \right) / I_i I_j \,, \tag{3.4}$$

and hence the whole inductance matrix.

3.2 Simulation Set-up[†]

The first task in the use of 3D-MLSI is to create the input file, which contains all the details about the system to simulate. The input file is simply a text file that can be created using a text editor (such as *Notepad* in Windows). 3D-MLSI is quite flexible in terms of the geometry of the components, but there are certain requirements that need to be satisfied by both the system and the input file. All the components of the system must be thin superconducting films. Once the height and thickness of each are defined, we consider their projection on the (*x*, *y*) plane; the boundaries of this projection are the subject of the input file. The films are separated by a perfect dielectric medium. The surface of a film can have arbitrary shape and contain holes and current terminals on its external boundary. The program assumes that the thickness of the film is small compared to its typical lateral size (i.e. the length or width of a strip or the side of a square washer) and of the same order as the penetration depth of the film.

Figure 3.3 below is an example of an input file, for a single strip (length 100μm, width 20μm, thickness 0.1μm, penetration depth 0.17μm) with two current terminals.

```
cc single strip, grds=1 [um] is multiplier for all sizes;

nc=1
ah=5
grds=1
lmbd=0.17

cond 0 -0.1 0.0


tp 1->2

ell 0 0   -20    0         0     0 t 1
ell 0 0     0    0         0   100
ell 0 0     0  100       -20   100 t 2
ell 0 0   -20  100       -20     0
```

Figure 3.3: example of an input file for 3D-MLSI.

[†] For the complete 3D-MLSI User's Manual refer to [20]

The first line in the file contains the name of the project and a comment ('*grds*' is a scaling factor: it defines the unit length of the quantities in the input file as a multiple of the micron. In this project, the unit length was always taken to be the micron so *grds* = 1). When the unit of length is 1μm, the calculated inductances are expressed in pH. The number of superconductors in the system must then be declared (*nc*). The command *ah* defines the resolution of the grid (roughly the linear size of the average mesh triangle), while *lmbd* is the London penetration depth of the film. In this project, the superconductors used in the simulations were usually assumed to be thin films of YBCO ($YBa_2Cu_3O_{7-x}$), which has parameters $\lambda_L(0) \cong 0.13\mu m$ [22] and $T_c \approx 88 \div 93K$ [3]. From equation (2.6), it follows that the penetration depth of YBCO at liquid nitrogen operating temperatures can be taken to be:

$$\lambda_{YBCO}(77K) \cong 0.23\mu m \tag{3.5}$$

Although this was the reference value adopted when simulating real magnetometers, other values were also employed and the dependence of the system parameters on penetration depth was explored.

3D-MLSI simulates inductances and current distributions for excitation currents circulating around holes or through chains of terminals. The algorithm for numerical solution requires boundary conditions, and these are in the form of terminals on the external boundary, or of holes within the conductor. This means that in order to obtain an inductance matrix there must be terminals and/or holes in the system. Terminals must always be in pairs (input and output terminal), so as to form terminal paths for the excitation currents to flow along. As mentioned before, they must lie on the external boundary of the superconductor. It is possible to set up chains of terminals rather than simply pairs. A more advanced option in 3D-MLSI allows the simulation of the current distribution given an external magnetic field or flux set by the user, in which case the program is unable to calculate the inductance matrix.

Each conductor is assigned a number and its thickness is fixed (refer to **Figure 3.3**). Each can have its own penetration depth and mesh resolution step (*ah*). The boundaries of the conductor are specified as linear elements: straight segments, arcs or circles. The command *ell* defines the geometrical form and features of the elements: origin and endpoint, centre, radius, etc. An element can be an edge, a terminal, or a hole boundary. **Figure 3.4** shows the input file for the simulation of a square washer and a source (a small strip). The elements that delimit a hole are labelled '*h i*' where *i* is the number of the hole, while terminal *n* is labelled '*t n*'. The command '*tp n* → *m*' sets the direction of flow of the current from terminal *n* to terminal *m*.

```
cc square washer, outer dimension D = 200 um, hole width d = 150 um;

nc=2
ah=5
grds=1.0
lmbd=0.17

cond 0 0 0.2

ell 0 0   -100  -100       100  -100
ell 0 0    100  -100       100   100
ell 0 0    100   100      -100   100
ell 0 0   -100   100      -100  -100
ell 0 0    -75   -75       -75    75 h 1
ell 0 0    -75    75        75    75 h 1
ell 0 0     75    75        75   -75 h 1
ell 0 0     75   -75       -75   -75 h 1

cond 1 0 0.2

tp 1->2

ell 1 0    499.5  -5       500.5  -5 t 1
ell 1 0    500.5  -5       500.5   5
ell 1 0    500.5   5       499.5   5 t 2
ell 1 0    499.5   5       499.5  -5
```

Figure 3.4: input file for the case of a square washer and a strip.

The input file can be opened with 3D-MLSI directly, for visualisation and execution of the pre-processor (the program UPM). UPM generates the mesh automatically, using one of the most recent and efficient finite element algorithms for mesh generation. The output from UPM is a file that constitutes the input of the numerical core (MLW), which is the most engaging part of the program in terms of CPU time. MLW produces two files: one containing all the information about the solution (including the current density at each node of the mesh, which is used to evaluate the inductance matrix but may not apply to a physical situation), and one containing the self- and mutual inductances in matrix form. The outcome of the simulation is immediately visualised in the program's window (WPM). It is possible to view the current distribution by displaying the streamlines and vanes indicating the trajectory and direction of flow, and by colour contrast, i.e. assigning a colour to each range of current density (see **Figure 3.5** below).

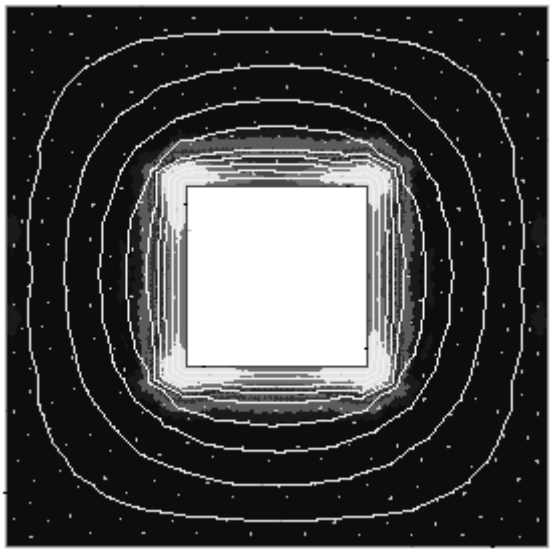

Figure 3.5: 3D-MLSI solution showing the current distribution and the streamlines.

3.3 Computational Goals and Tools

The main objective of this project was to understand how 3D-MLSI is to be used in the design of real SQUID sensors. For this purpose, one needs to elucidate the details of the program and work out how the information about a device must be inserted and extracted from the code. For example, how is a Josephson junction to be modelled? What is the equivalent inductance of a SQUID circuit? As the details of the apparatus that are entered into the program are of essentially two natures only (geometrical and boundary conditions-like), and because the output is a somewhat obscure matrix containing the inductances of the current paths rather than of the actual components of the system, the data that we get from 3D-MLSI has to be analysed and processed before it can give us any useful information. At the same time, the accuracy of the method is intrinsic to the numerical technique used to solve the relevant equations, and so it lies on the resolution of the mesh rather than on experimental conditions. These issues call for a test of the validity and precision of the computational method, which can come from either theory or experiment. So before investigating real, interesting designs, an analysis of the characteristics and limitations of the code was carried out on simple systems, such as striplines and square washers, of which the specifications were known. Moreover, in discussing the results, the data obtained from 3D-MLSI has been compared to analytical formulae or experimental data whenever these were available.

3.3.1 Superconducting strip

The simplest superconducting system is a single thin stripline. Because of its elementary geometry, it has been studied extensively from both a theoretical and experimental point of view, so it is the perfect tool to investigate the validity and accuracy of 3D-MLSI. In the present project, a stripline has been used to investigate mesh resolution effects, the dependence of inductances on penetration depth and the dependence of mutual inductance on the distance between two superconductors. A stripline was also used as the magnetic field source when studying the effective area of a magnetometer.

The inductance of a superconducting strip has a magnetic and a kinetic term. The kinetic inductance for such a geometry cannot be neglected, because the strip cross-section is comparable to the square of the penetration depth. We can see why this characteristic is important by considering the analytical form of the kinetic inductance of a strip of length ℓ, width w and thickness t [4]:

$$L_k = \frac{\mu_0 \lambda_L^{\,2} \ell}{wt} \tag{3.6}$$

For a typical stripline with a ratio $\ell/w \gtrsim 10$, and thickness and penetration depth of a few tenths of microns (which is the case for YBCO thin films), the kinetic inductance is greater than or in the order of a few tenths of pH. It will become apparent in the course of this report that this value can affect the accuracy of the result, and therefore should always be taken into account. This consideration also applies to the more complex geometries considered hereafter.

As for the magnetic term of the inductance, we can turn to classical electromagnetic theory (in which the kinetic inductance is not predicted) for analytical formulae. For normal conductors and in the absence of magnetic materials, the mutual and self-inductance are parameters that do not depend on the current distribution but only on the geometry, so long as we can neglect skin depth effects (which are only important in high-frequency situations) [21]. Although superconductors are perfect *bulk* diamagnets (i.e. they have zero *global* permeability μ_r) because of the Meissner effect, their *local* permeability is close to 1, as for normal non-magnetic materials [23]. Moreover, given the low fields in which SQUIDs operate (below B_{c1}), the magnetic inductance should be independent of field and current. If these two assumptions are true, the formulae for the magnetic inductance of normal conductors must hold for superconductors as well. Because nothing was found

in the literature to clarify this issue, 3D-MLSI was used to compare computational data with predictions of self-inductance from normal conductors.

The magnetic inductance of a stripline of length ℓ, rectangular cross-section and small shape ratio (i.e. width $w \gg$ thickness t) is [21]:

$$L_m = 0.2\ell\left[\ln\frac{2\ell}{w+t}+\frac{1}{2}\right] \tag{3.7}$$

where L has units of pH when ℓ is expressed in microns. If the same approximations adopted for equation (3.6) hold true, the magnetic inductance of the strip will be of a few tens of pH.

3.3.2 Square washer

The square washer is the most common design for pickup loops in SQUID magnetometers and has been studied extensively. Jaycox and Ketchen [10] have shown that a square washer with outer dimension D and hole width d has a self-inductance approaching the value $L = 1.25\mu_0 d$ when the width of the loop $W = (D-d)/2$ becomes on the order of or greater than d. Also, Ketchen et al [6] have shown that the effective area of the washer is $A_{eff} = aDd$, where a is a numerical constant of order unity. The computational method in 3D-MLSI has been tested against these results [13], showing, for the case of the self-inductance, accuracy of about 2-3%. Those calculations were repeated in the present project, and extended to the case of the effective area. The investigation on square washers was the taken further, with studies of the dependence of the inductances on penetration depth (an almost impossible task to do experimentally) and of the variation of mutual inductance between a washer and a source as a function of distance between the two (measured from the centre of the washer hole to the vertical axis of the strip, see **Figure 3.6** below).

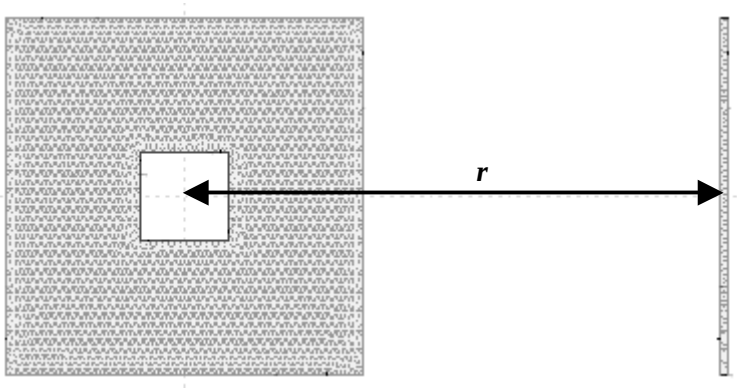

Figure 3.6: square washer and source in the shape of a stripline, r = 200μm apart.

Actual square washer pickup loops have slits that contain the Josephson junctions [1] (refer to **Figure 3.7** and **3.8** below). The presence of a slit will modify the field and current distribution on the washer [6], though the effect on the inductances is usually neglected. The result of including a slit in a square washer was considered, by making the slit width vary until it approached zero, and then comparing with a square washer with no slit. A convergence to the value for the washer with no slit was expected. In using 3D-MLSI, there is a significant difference between simulating a washer with slit and no slit. For the latter case, the boundary conditions are provided by the presence of the hole, whereas for the former case, the presence of a terminal path is required. The choice of location and width of the terminals is a crucial one, for the terminals are an artificial imposition to the physical system and could affect the current distribution arbitrarily.

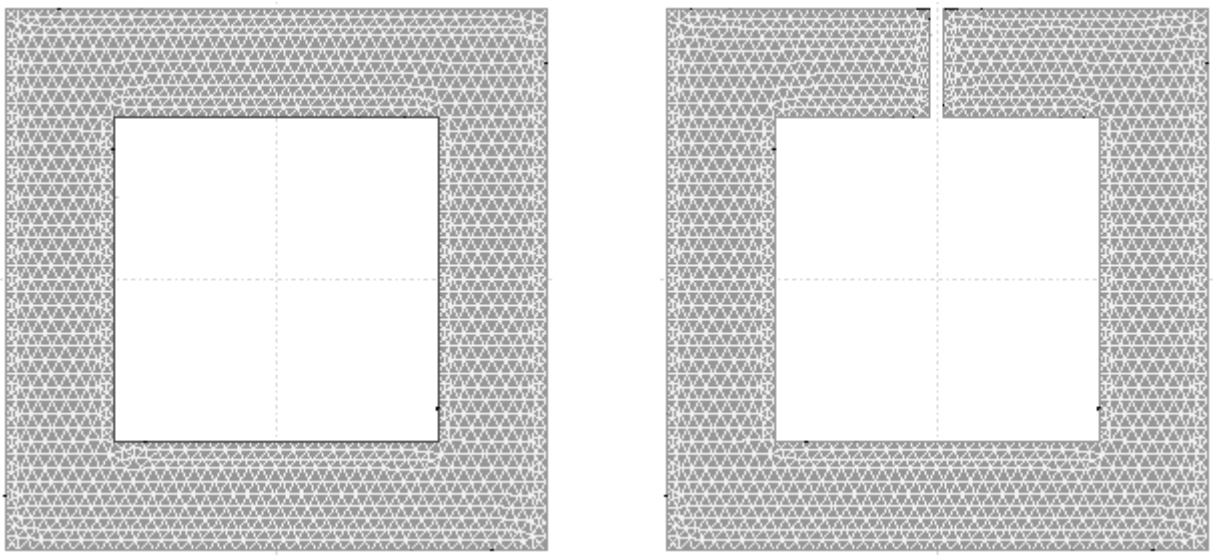

Figure 3.7: visual comparison between a square washer without a slit and another with a 1μm-wide slit.

3.4 Kahlmann's SQUID

A device of particular interest is the magnetometer layout introduced by Lee et al [24], [25] and developed by Kahlmann et al [26], which for convenience will be hereafter referred to as *Kahlmann's SQUID*. It consists of a directly coupled magnetometer where the pickup loop is in the form of a square washer (see **Figure 3.8** below). Kahlmann et al have measured the effective area of the device, so it was decided to compare those results with calculations using 3D-MLSI.

The magnetometers in [26] were patterned out of 200nm thick YBCO films. The square pickup loop has an outer dimension of 2mm and a width of 0.75mm, while the hole has a side 0.5mm long. The SQUID loop is placed within the square washer, it has a linewidth of 4μm and the two strips are 5μm apart. The length of the SQUID loop is varied to obtain four values of the SQUID inductance, 50pH, 100pH, 150pH and 200pH (for simplicity, the magnetometers will be labelled according to their respective SQUID inductance value).

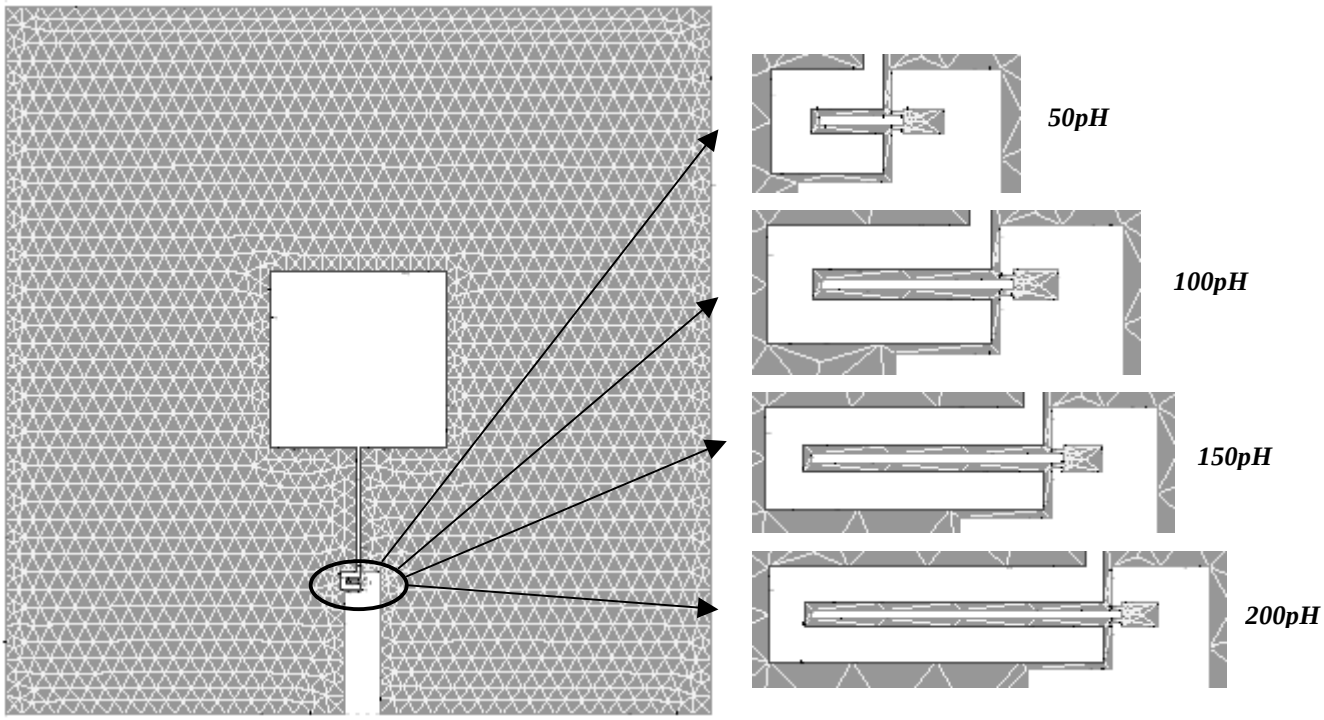

Figure 3.8: Kahlmann's SQUID. The pickup loop is common for all magnetometers (left). The length of the SQUID is tuned to obtained the desired SQUID self-inductance, as shown by the four enlargements on the right.

The system has four components: the pickup loop, the two parts of the SQUID separated by the Josephson junctions and the source (a long and narrow strip, which can be considered as a

current dipole). Thus the inductance matrix will be a 4×4 matrix and the information about the equivalent inductances of the circuit must be extracted for the specific purpose. The method that has been employed is a special case of the method discussed in [17]. We start with the statement that the vector $\mathbf{\Phi}$ of fluxoids trapped in holes or excited by terminal currents is given by:

$$\mathbf{\Phi} = L\mathbf{I} \tag{3.8}$$

where $\mathbf{I} = \left(I_1,...,I_{N_h}, I_{N_h+1},...,I_{N_h+N_t}\right)$ is the vector of full currents circulating around holes and through terminals, while L is the inductance matrix. It is recalled that L is an $N\times N$ symmetric positive-definite matrix, and $N = N_h + N_t$. For $i = 1,...,N_h$ the vector component Φ_i is the fluxoid trapped in hole i, while for $i = N_{h+1},...,N_h + N_t$ the component Φ_i is the sum of fluxoids for a given sequence of terminals on a superconductor. Because in 3D-MLSI the currents circulating around holes are excited by externally applied currents (the terminal currents), the self- and mutual inductance terms associated with holes are dependent on the terms due to terminal currents, and so the inductance matrix can be effectively reduced in size. If we decompose the vectors of fluxoids and of currents into sub-vectors $\mathbf{\Phi}^{(1)} = \left(\Phi_1,...,\Phi_h\right)$ and $\mathbf{I}^{(1)} = \left(I_1,...,I_h\right)$ of length $h = N_h$, and sub-vectors $\mathbf{\Phi}^{(2)} = \left(\Phi_{h+1},...,\Phi_N\right)$ and $\mathbf{I}^{(2)} = \left(I_{h+1},...,I_N\right)$ of length $l = N_t$, equation (3.8) can be rewritten as:

$$\begin{pmatrix}\mathbf{\Phi}^{(1)}\\ \mathbf{\Phi}^{(2)}\end{pmatrix} = \begin{bmatrix}L_{11} & L_{12}\\ L_{21} & L_{22}\end{bmatrix}\begin{pmatrix}\mathbf{I}^{(1)}\\ \mathbf{I}^{(2)}\end{pmatrix} \tag{3.9}$$

where L_{11}, L_{12}, L_{21} and L_{22} are sub-matrices of L with dimensions $h\times h$, $h\times l$, $l\times h$ and $l\times l$ respectively. Solving for $\mathbf{\Phi}^{(1)}$ in terms of $\mathbf{\Phi}^{(2)}$, we obtain the following relation:

$$\mathbf{\Phi}^{(2)} = \tilde{L}\mathbf{I}^{(2)} + L_{21}{L_{11}}^{-1}\mathbf{\Phi}^{(1)} \tag{3.10}$$

where

$$\tilde{L} = L_{22} - L_{21}{L_{11}}^{-1}L_{12} \tag{3.11}$$

is the reduced inductance matrix of the system, having dimensions *l*×*l*. Note that $\tilde{L}$ is symmetric as L_{11} and L_{22} are symmetric and $L_{21} = L_{12}^{T}$. Now, the flux trapped in the hole of a superconductor is quantised and constant. If we consider the fact that SQUID magnetometers are used to measure very small magnetic signals, given the low intensity of the fields in which they operate we can safely assume that no flux is trapped in the holes and the elements of $\mathbf{\Phi}^{(1)}$ can be taken to be zero. Equation (3.10) then reduces to:

$$\mathbf{\Phi}^{(2)} = \tilde{L}\mathbf{I}^{(2)} \tag{3.12}$$

In our specific case, the indices 1, 2, 3 and 4 denote the pickup loop, the section of the SQUID connected to the pickup loop, the other part of the SQUID and the source respectively. We can reduce the 4×4 inductance matrix to a 3×3 matrix, using $\tilde{L}$. Our basic assumption for the solution of this problem is that the currents through the terminal paths on the two sections of the SQUID (I_2 and I_3) are equal. This is because we are modelling a pair of Josephson junctions connected in parallel on a closed loop, so the same supercurrent must go through both (the bias current contributes nothing to the inductance so it is ignored). Sub-vector $\mathbf{I}^{(2)}$ can be written as (I_2, I_2, I_4) and equation (3.12) yields the system of linear equations:

$$\begin{cases} \Phi_2 = \left(\tilde{L}_{11} + \tilde{L}_{12}\right)I_2 + \tilde{L}_{13}I_4 \\ \Phi_3 = \left(\tilde{L}_{12} + \tilde{L}_{22}\right)I_2 + \tilde{L}_{23}I_4 \\ \Phi_4 = \left(\tilde{L}_{13} + \tilde{L}_{23}\right)I_2 + \tilde{L}_{33}I_4 \end{cases} \tag{3.13}$$

The flux threading the SQUID (which is the quantity measured by the device) is the sum of the fluxes linking its two components (see **Figure 3.9** below):

$$\Phi_{SQUID} = \Phi_2 + \Phi_3 = \left(\tilde{L}_{11} + 2\tilde{L}_{12} + \tilde{L}_{22}\right)I_2 + \left(\tilde{L}_{13} + \tilde{L}_{23}\right)I_4 \tag{3.14}$$

It is straightforward now to calculate the equivalent mutual and self-inductance of the magnetometer from equation (3.14). The equivalent self-inductance L_{eq} is found by imposing $I_4 = 0$ and by dividing the flux through the SQUID by the current flowing in it:

$$L_{eq} \equiv \left. \frac{\Phi_{SQUID}}{I_2} \right|_{I_4=0} = \tilde{L}_{11} + 2\tilde{L}_{12} + \tilde{L}_{22} \tag{3.15}$$

Similarly, the equivalent mutual inductance between Kahlmann's magnetometer and the source is:

$$M_{eq} \equiv \left. \frac{\Phi_{SQUID}}{I_4} \right|_{I_2=0} = \tilde{L}_{13} + \tilde{L}_{23} \tag{3.16}$$

Note that when considering the equivalent self-inductance of a circuit, which is an intrinsic property of the system of conductors, the value of the coupling current in the source should by no means affect the result; hence the assumption $I_4 = 0$ in (3.15). Moreover, the mutual inductance is a measure of the coupling between two loops; it relates the current through one to the induced currents through the other and so any externally injected current in the second loop (e.g. I_2 for the magnetometer) does not enter the picture of mutual inductance and should be neglected. This argument justifies the assumption $I_2 = 0$ in (3.16).

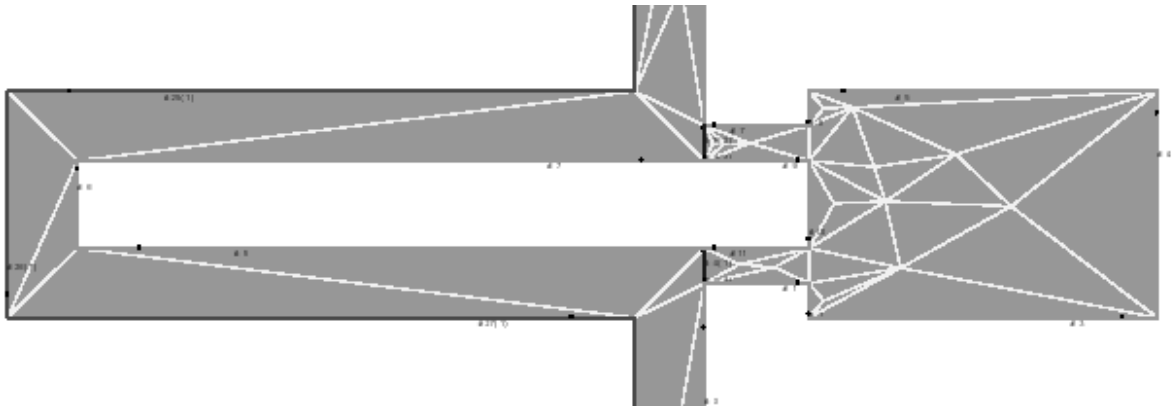

Figure 3.9: the flux measured by the SQUID is the flux linking the slit. This flux is the sum of two components: that from the hairpin-shaped loop on the left, and that from the component to the right. The blue vertical segments are the terminals, which effectively simulate the Josephson junctions.

If we consider a system with only three components (the pickup loop, the SQUID and the source), it can be shown by the same procedure that the equivalent mutual inductance between the magnetometer and the source is:

$$M_{eq} = M_S + \frac{L_S}{L_p} M_p \tag{3.17}$$

where M_S and M_p are the mutual inductance between source and SQUID, and source and pickup loop respectively, L_S is the self-inductance of the SQUID and L_p the self-inductance of the pickup loop. If we multiply both sides of equation (3.17) by $4\pi r^2 / \mu_0 \ell$ and then take the limit as $r \to \infty$, according to equation (2.21) we get the effective area of the magnetometer. It is straightforward to verify that the formula for the effective area thus obtained is the same as equation (2.20).

The procedure for extraction of the equivalent SQUID self-inductance is simpler than for the whole magnetometer. There are only two components: the two loops connecting the junctions. The current circulating around the coil is *I*, the fluxes are then given by:

$$\begin{pmatrix} \Phi_1 \\ \Phi_2 \end{pmatrix} = \begin{bmatrix} L_{11} & L_{12} \\ L_{12} & L_{22} \end{bmatrix} \begin{pmatrix} I \\ I \end{pmatrix} \tag{3.18}$$

The total flux threading the SQUID is the sum of the two fluxes in (3.18), so the equivalent self-inductance is simply:

$$L_{eq} \equiv \Phi_{SQUID} / I = L_{11} + 2L_{12} + L_{22} \tag{3.19}$$

4. Results

Before using the software to study complex and interesting systems, the properties and limits of 3D-MLSI were investigated. In particular, emphasis was laid on the accuracy of the method by varying the resolution step and observing the evolution of the outcome. It was also checked that the inductances and effective areas had the expected dependence on penetration depth and distance from the source. Some analytical and experimental values were available for comparison, but while formulas and empirical data are abundant as far as the inductance is concerned, for the effective area scarce information could be found in the literature.

4.1 Effect of mesh size

The first step in the project was to study the effect of mesh resolution on the inductance matrix. Because finite element techniques are numerical methods based on discretisation of continuous systems, they are valid strictly in the limit that the grid elements tend to infinitesimal entities. Thus we expect our results to be only crude estimates that tend asymptotically to the exact value, but nevertheless they should be reliable to a certain degree. Just how reliable is a question that requires an answer in the framework of this project.

For simplicity, the first choice for a test superconductor was a thin strip (100μm long, 14μm wide and 0.2μm thick). The penetration depth used was 0.135μm, which is the value for YBCO at absolute zero [3] (the penetration depth dependence of the inductance will be dealt with later in this chapter).

(a) (b)

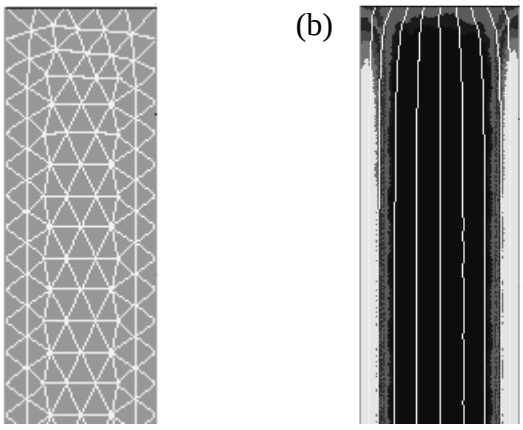

Figure 4.1: section of the strip showing the triangular mesh (a) and the current distribution (b). The mesh size is $ah = 3$. The colour scheme in (b) is a measure of the current density, from blue (lowest) to yellow (highest).

Figure 4.1 shows the strip after the pre-processor run (a) and after the numerical core (b): it exhibits the grid on the left and the current distribution on the right. The resolution step is 3 for this case. For visual comparison, the same system but with a lower mesh resolution (*ah* = 10) has been presented below (**Figure 4.2**). It is evident that the mesh is much coarser, and accordingly the current distribution is asymmetric and incoherent. The different colours represent different values of the current density, from yellow (highest) to dark blue (lowest). In **Figure 4.1** the current is concentrated along the borders of the strip, decreasing exponentially as we move inwards, in agreement with the Meissner effect. The strip in **Figure 4.2**, on the other hand, is so deeply affected by the coarseness of the grid that the current distribution appears random, dictated by the large area of the triangles (the sides of which are of the same order as the width of the strip). The obvious conclusion is that the resolution step must be much smaller than the dimensions of the superconductor, otherwise finite size effects become dominant and the simulation looses physical significance.

(a) (b)

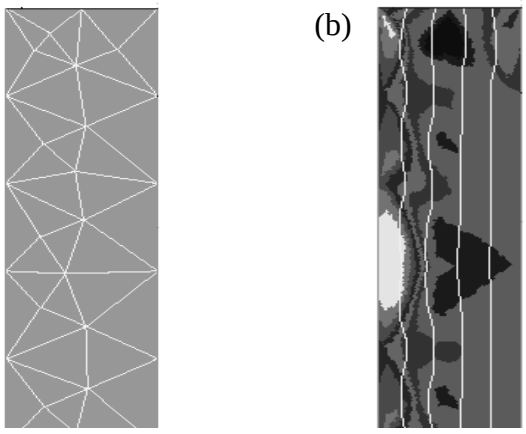

Figure 4.2: section of the strip showing the triangular mesh (a) and the current distribution (b). Mesh size is now 10. The accuracy and symmetry of the current distribution is suffering from the poor resolution of the mesh.

The effect of mesh resolution on the inductance can be appreciated in **Figure 4.3** below. The asymptotical behaviour of the self-inductance as the mesh is refined is apparent, but interestingly enough the inductance experiences an *overestimation* that grows as *ah* increases. There is thus a definite correlation between the size of the triangles and the total energy of the system (from which the inductance matrix is found).

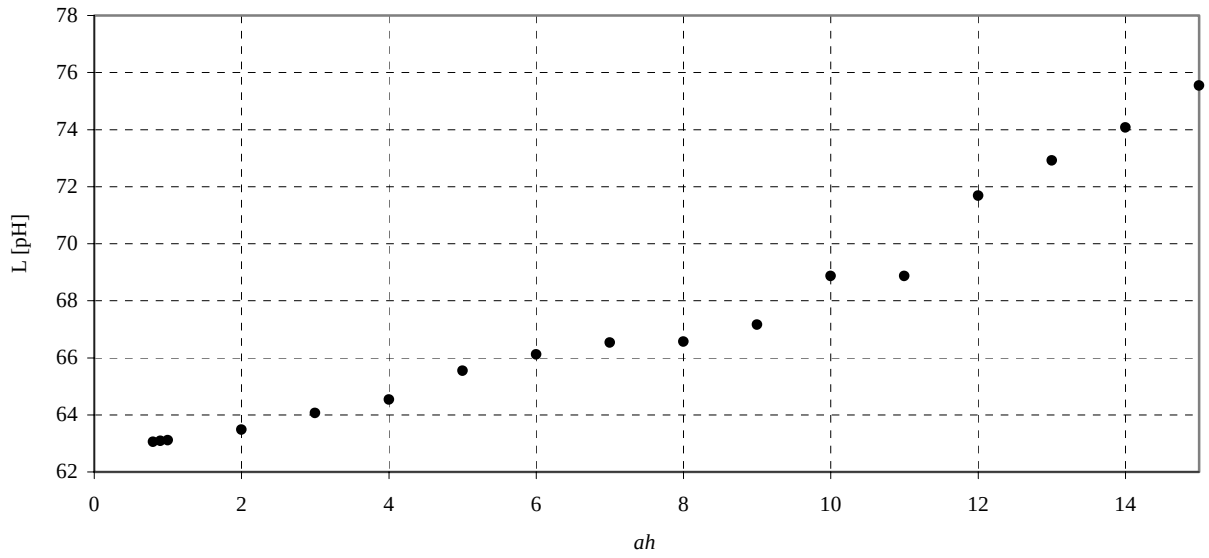

Figure 4.3: self-inductance of the strip as a function of mesh size *ah*.

The self-inductance of the strip seems to converge to approximately 63pH. It will be shown in the next section that this result is consistent with theoretical predictions. Note that all values are within 20% of the lowest value (63.05pH for *ah* = 0.8). In particular, for a resolution step smaller in size than 10% of the strip width (i.e. for *ah* < 2) the overestimation is below 1%. So the mesh size can be "tuned" so as to give the required accuracy, given that precision has a cost in terms of computer power time and memory. For example, CPU time was 5.0 s when *ah* = 3, 1.0 s when *ah* = 5 and less than 0.1 s when *ah* = 10 (the simulations in this project were performed with an Intel® Celeron™ 600 MHz processor and a 192 MB RAM).

4.2 Effect of penetration depth on stripline inductance

The effect of penetration depth on the stripline self-inductance was discussed in section 3.3.1, where the kinetic inductance was shown to be proportional to $\lambda_L^{\,2}$, while the magnetic inductance was taken to depend on the geometry only. The same considerations are expected to apply to the mutual inductance between two superconductors as well. For the strip considered in section 4.1, formula (3.6) for the kinetic inductance and formula (3.7) for the magnetic inductance, yield $L_k = 44.88\lambda_L^{\,2}\ pH/\mu m^2$ and $L_m = 62.90\,pH$ respectively.

Figure 4.4 is a plot of the self-inductance of the same superconducting strip of section 4.1, as a function of the square of the penetration depth. The mesh size used was 5. If our predictions are correct, i.e. if the kinetic inductance is accurately given by equation (3.6) and the magnetic inductance depends only on geometry, we expect a plot of the total inductance minus the kinetic inductance to be a horizontal line with a y-intercept at approximately 63pH.

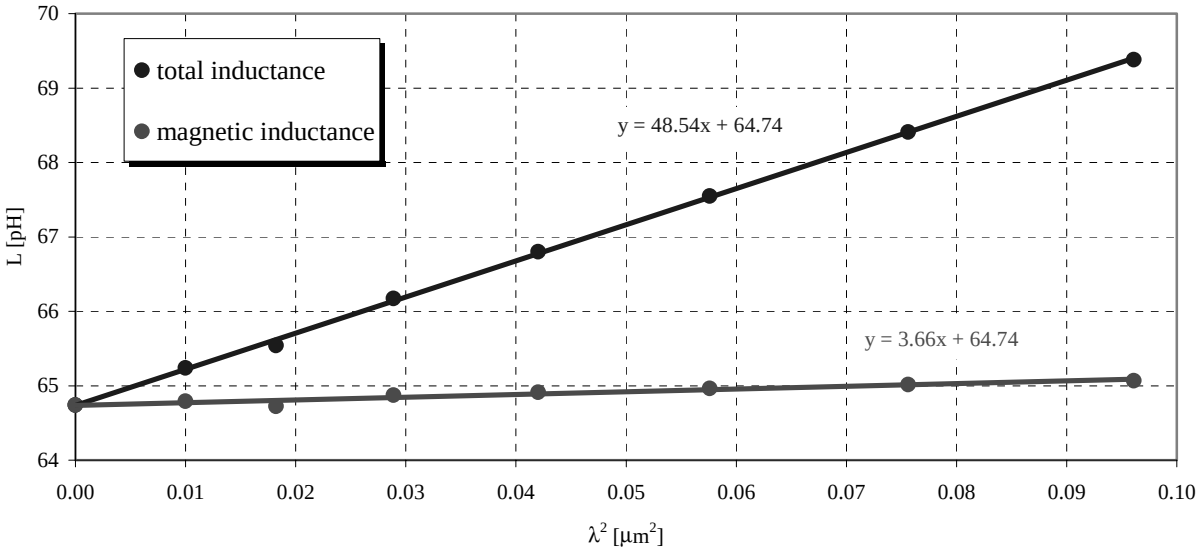

Figure 4.4: self-inductance of the strip as a function of penetration depth.

The blue trendline in **Figure 4.4** shows that the self-inductance of the stripline is indeed proportional to $\lambda_L^{\,2}$. The y-intercept is the magnetic inductance of the strip (the kinetic term is zero when λ_L is zero), and the value 64.74pH is in good agreement (3%) with the prediction of 62.90pH from equation (3.7), considering the overestimation due to mesh resolution (ah = 5 in this case). The slope of the trendline is $L_k / \lambda_L^{\,2}$, and there is an 8% mismatch between 3D-MLSI's result ($48.54\, pH/\mu m^2$) and the theoretical prediction from equation (3.6) ($44.88\, pH/\mu m^2$). Again, we may put this down to mesh resolution, although the effect in this case is more dramatic. Similarly, by taking the predicted value of the kinetic inductance for a given λ_L out of the total self-inductance, we obtain a quantity which is still penetration depth dependent. If the magnetic inductance depends entirely on geometry, this implies a general overestimation of the kinetic inductance, which is a logical conclusion given the results of section 4.1. It would therefore not seem unreasonable to support the hypothesis that magnetic inductance is not affected by the current

distribution, though of course more experimental evidence is needed to reach a decisive conclusion on the subject.

4.3 Square washer

To test the accuracy of 3D-MLSI, the inductance of a square washer with a hole was compared with the value found by Jaycox and Ketchen, $L = 1.25\mu_0 d$ [10], where d is the width of the hole. The devices in [10] were made of low-T_c superconductors, so the value of the penetration depth was chosen to be 50nm (which is the right order of magnitude for e.g. Nb). A plot of $L/\mu_0 d$ against W/d, where W is the width of the loop, for three different hole widths is compared with the original data from [10] in **Figure 4.5** below.

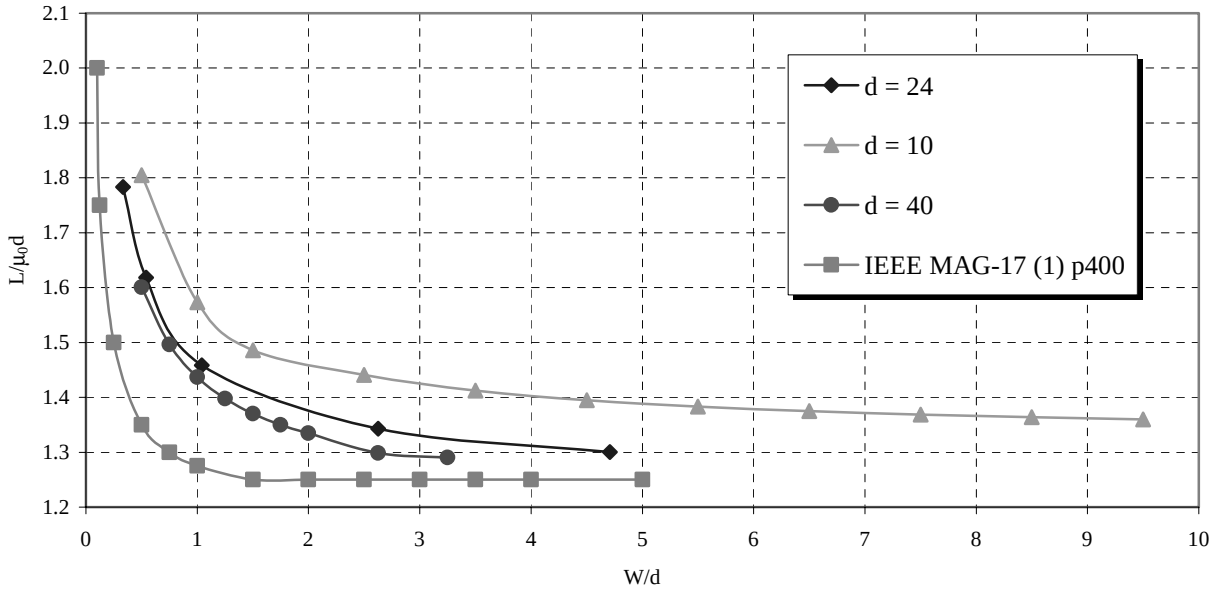

Figure 4.5: graph of $L/\mu_0 d$ vs. W/d for three different hole widths d and the expected curve from [10].

The three curves in **Figure 4.5** seem to settle at a limiting value between 1.4 and $1.2\,\mu_0 d$. This is consistent with a prediction of 1.25 (once again, the overestimation effect must be taken into account). The shape of the curves is in good agreement (less than 10% mismatch) with the result presented by Jaycox and Ketchen only for d = 24μm and d = 40μm and when $W \gtrsim d$. The agreement increases significantly though (less than 3% error) for the blue and the red curve when $W \gtrsim 2d$. This

implies that for large washers with large *W*/*d* values (which is usually the case for actual SQUID magnetometers), 3D-MLSI produces an accurate and reliable result. Unfortunately, probing the inductance of square washers with hole widths greater than 10 beyond a ratio *W*/*d* of 5 proved to be impossible for a resolution step of 5. When the number of mesh points exceeds an upper limit, the power of the processor becomes inadequate to run the program and 3D-MLSI is unable to perform its tasks. For example, in the case d = 40μm and D = 300μm, the CPU time was 2907 s. Trying to increase D was not possible with the 600 MHz processor. Nevertheless, it was deemed necessary to maintain a high resolution in order to reproduce the result of [10].

Note that the value of $L/\mu_0 d$ decreases as d increases. This is due to the fact that while the resolution step is kept fixed (ah = 5), the relative resolution improves as the washer size (and thus d) increases, and we have seen that poorer resolution results in a greater overestimation of the inductance.

The effective area is an intrinsic property of a loop, so we expect it to be constant (at least asymptotically) as the distance between the loop and the source increases. The effective area was considered in section 2.3.2, where it was shown that using a strip as a source at large distances (so that the magnetic field becomes uniform) it can be obtained from:

$$A_{eff} = \lim_{r\to\infty}\frac{\Phi}{B} = \lim_{r\to\infty}\frac{MI}{\left(\mu_0 \ell I/4\pi r^2\right)} = \lim_{r\to\infty}\frac{4\pi}{\mu_0}\frac{Mr^2}{\ell} \tag{2.21}$$

In (2.21), r is the distance between washer and source and ℓ the length of the strip that acts as a source. If the mutual inductance is then inversely proportional to the square of distance (at least for large values of r), the effective area will approach its limiting value. For verification, the mutual inductance between a square washer and a strip was investigated, varying the distance between the two. The square washer had parameters: D = 200μm and d = 50μm. The stripline was 100μm long and 5μm wide. The thickness and penetration depth of both conductors were chosen to be 0.2μm. The effective area was expected to be roughly 0.01mm^2 from the formula $A_{eff} \approx dD$ in [6]. The resolution step was 5.

The assumptions on the mutual inductance and the effective area are confirmed by **Figure 4.6** and **Figure 4.7**. The effective area appears to be approaching a value roughly in the range 0.00912÷0.00914mm^2.

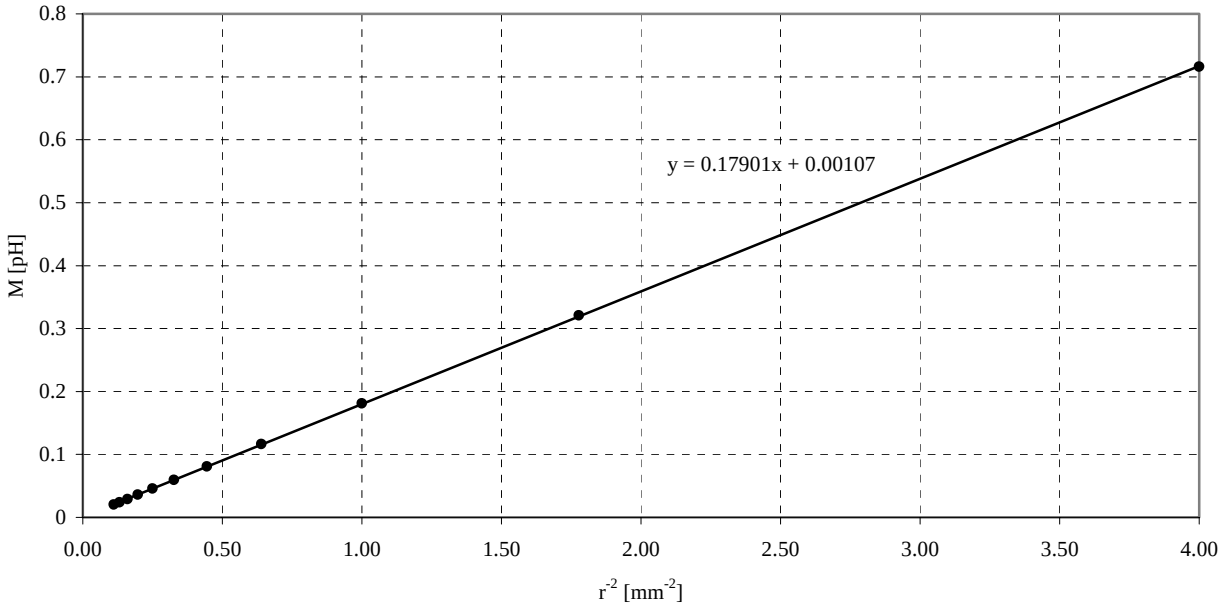

Figure 4.6: mutual inductance between washer and source as a function of r^{-2}. The datapoints are well fitted by a straight line, indicating that $M \propto r^{-2}$.

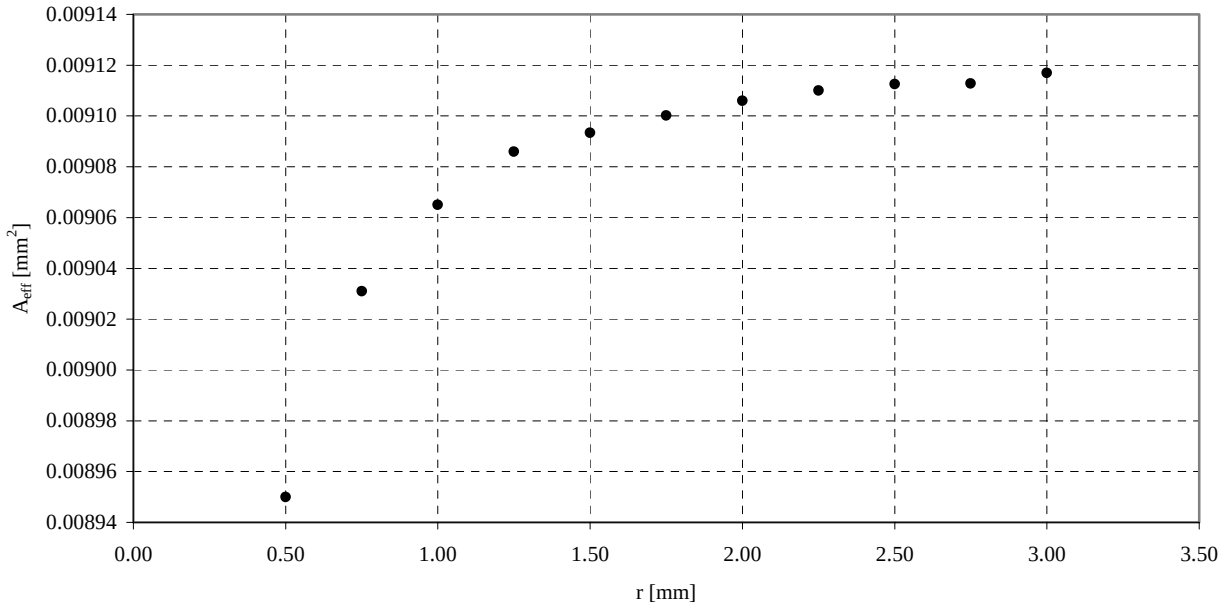

Figure 4.7: effective area of the square washer as a function of distance from source. The curve seems to be approaching a limiting value of $0.00912 \div 0.00914 mm^2$.

Once established that the effective area reaches its limiting value for distances $r \gtrsim 2\text{mm}$, the data obtained from 3D-MLSI and equation (2.21) were compared with the result $A_{eff} \approx dD$ from [6]. A number of square washers of different dimensions were simulated, using a strip of length equal to the outer dimension D and width 5μm as a source. The distance between the two conductors was 2mm. The effective area of the square washers found using 3D-MLSI and equation (2.21) is shown in **Figure 4.8**, as a function of dD.

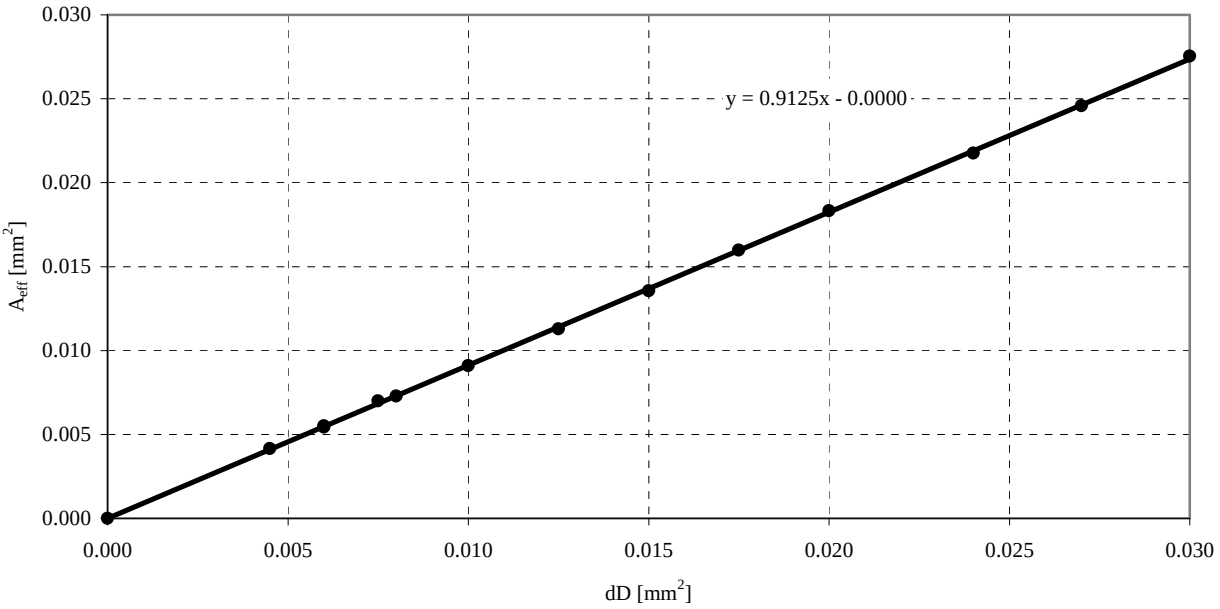

Figure 4.8: effective area of square washer obtained via 3D-MLSI and equation (2.21) as a function of dD.

The datapoints in **Figure 4.8** show that the effective area is proportional to the quantity dD. The constant of proportionality, 0.9125, is of the order unity, as predicted by Ketchen et al [6].

It was then decided to study the behaviour of the square washer inductances when the penetration depth was varied. For that purpose, a washer with outer dimension D = 200μm, hole width d = 50μm and thickness t = 0.2μm was coupled to a stripline source (10μm long, 5μm wide, 0.2μm thick and with a penetration depth of 0.2μm) in order to compute the mutual and self-inductance. The penetration depth of the square washer was sampled between 0 and 50μm. Although in reality λ_L ranges from a few tens to a few hundreds of nanometers, this choice was made to probe the response of 3D-MLSI to situations beyond the expected range of validity. The resolution step was once more taken to be 5.

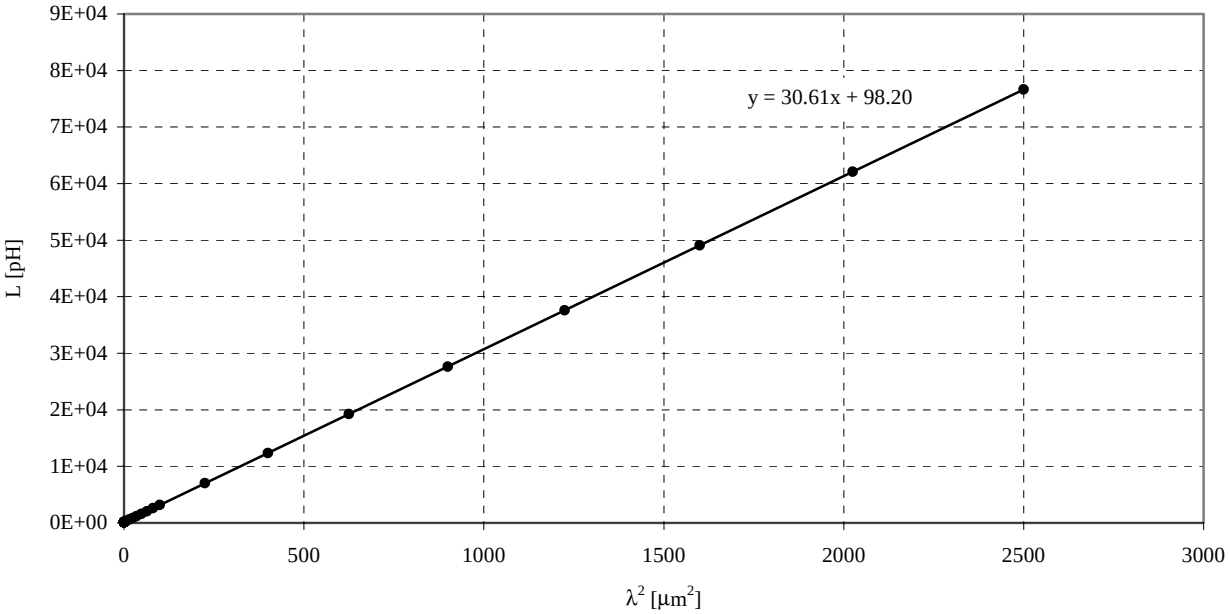

Figure 4.9: self-inductance of the square washer as a function of the square of penetration depth.

Like for the stripline of section 4.2, the inductance of the square washer has a square dependence on the penetration depth (as shown by the straight line fitting the points in **Figure 4.9**, which is a graph of the self-inductance against $\lambda_L^{\,2}$). This is hardly surprising if we consider the definition of the kinetic energy of a supercurrent [11], reproduced in equation (2.22). The slope of the fit in **Figure 4.9** ($30.61 pH/\mu m^2$) is the kinetic inductance per $\lambda_L^{\,2}$ of the washer, while the y-intercept ($98.20 pH$) is the washer's magnetic inductance. If we compare the value of $L_k / \lambda_L^{\,2}$ extrapolated from the graph, with that of a stripline of identical dimensions calculated using equation (3.6), which in this case yields 41.89 $pH/\mu m^2$, we see that there is a 40% discrepancy between the two. It follows that we cannot use the kinetic inductance per unit length of a stripline to approximate the kinetic inductance per unit length of a square washer loop.

If we consider the mutual inductance between the washer and a source, the dependence on penetration depth shows quite a different pattern, as we can see from **Figure 4.10** below:

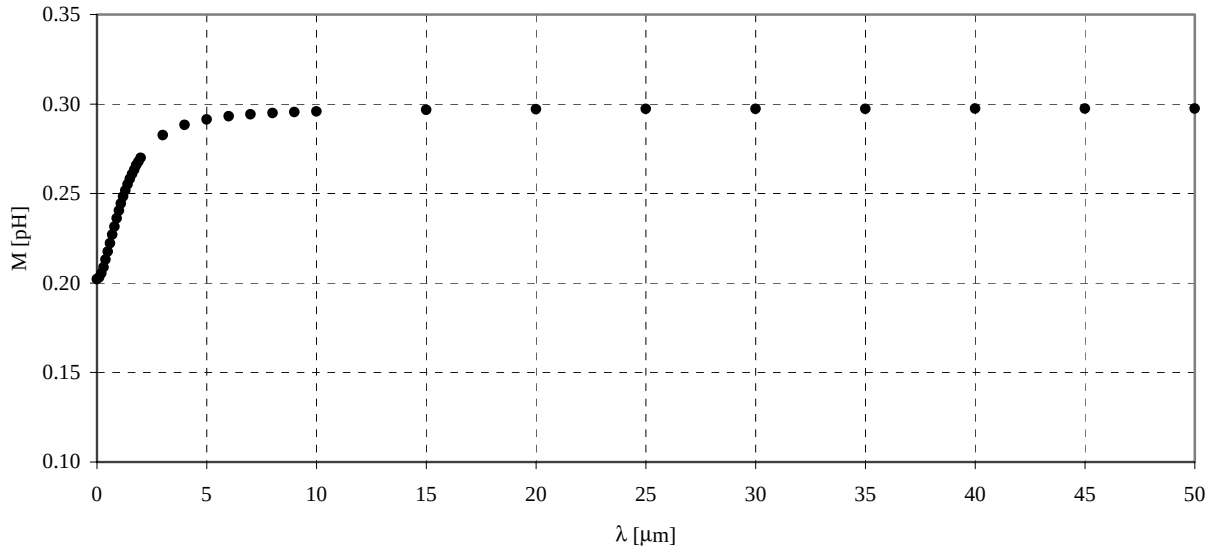

Figure 4.10: mutual inductance between washer and source as a function of the square of penetration depth.

The mutual inductance seems to increase parabolically at first (see **Figure 4.11** below), but then it approaches a constant value of approximately 0.3pH. This peculiar feature might be explained as follows. The current distribution on the washer is typical of superconductors at small values of penetration depth, with screening currents flowing along the edges. As λ_L increases, the zero-current zero-field region gets narrower as the screening currents are spread over a larger area. At some point, the screening currents meet and the current distribution becomes uniform, like for a normal conductor (for which the penetration depth can be considered to be infinite [3]). As a result (when the penetration depth becomes of the same order as half the width of the loop) there are no more changes to the current distribution and thus to the total energy of the system.

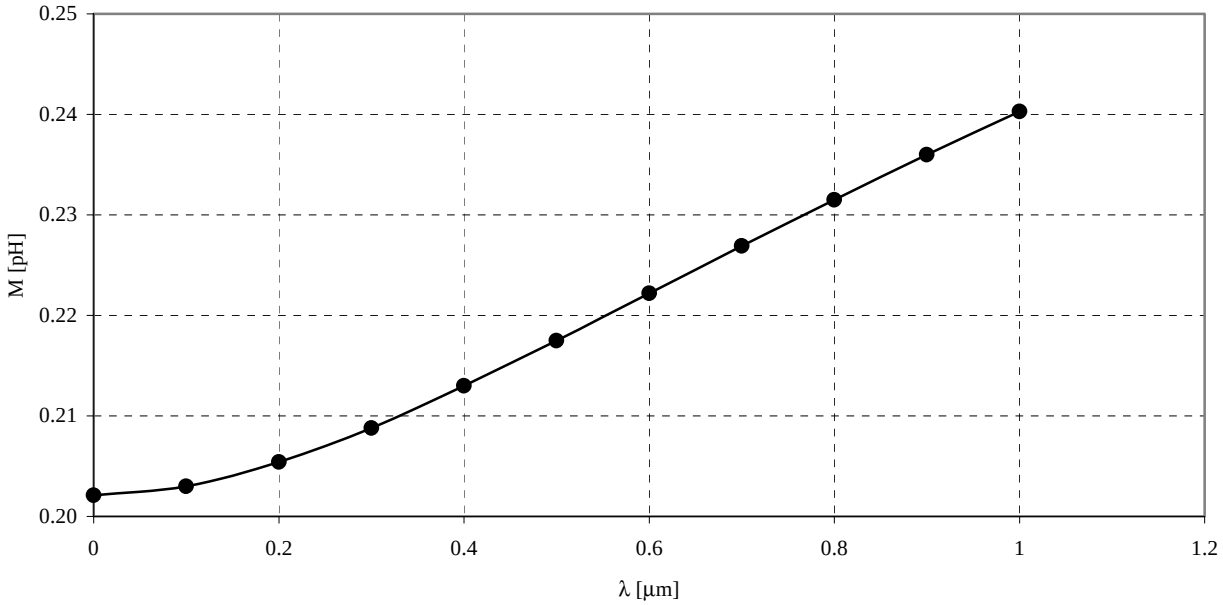

Figure 4.11: detail of the graph in Figure 4.10 showing the λ-dependence of M for small values of λ.

The final investigation into the behaviour of square washer was the comparison of washers with slits and washers without. In reality, square washer pickup loops are slitted so that the SQUID can be placed in the slit [1]. Nevertheless, the contribution of the slit to the total inductance is for simplicity neglected (see e.g. [6]) and the parameters of the pickup loop are taken to be those discussed for the square washer without a slit. This assumption was tested using 3D-MLSI. A square washer (D = 40μm, d = 24μm, t = 0.2μm and λ_L = 0.05μm) was simulated without a slit and with a number of slits of different widths connecting the hole to the external edge. The results are shown in **Figure 4.12**.

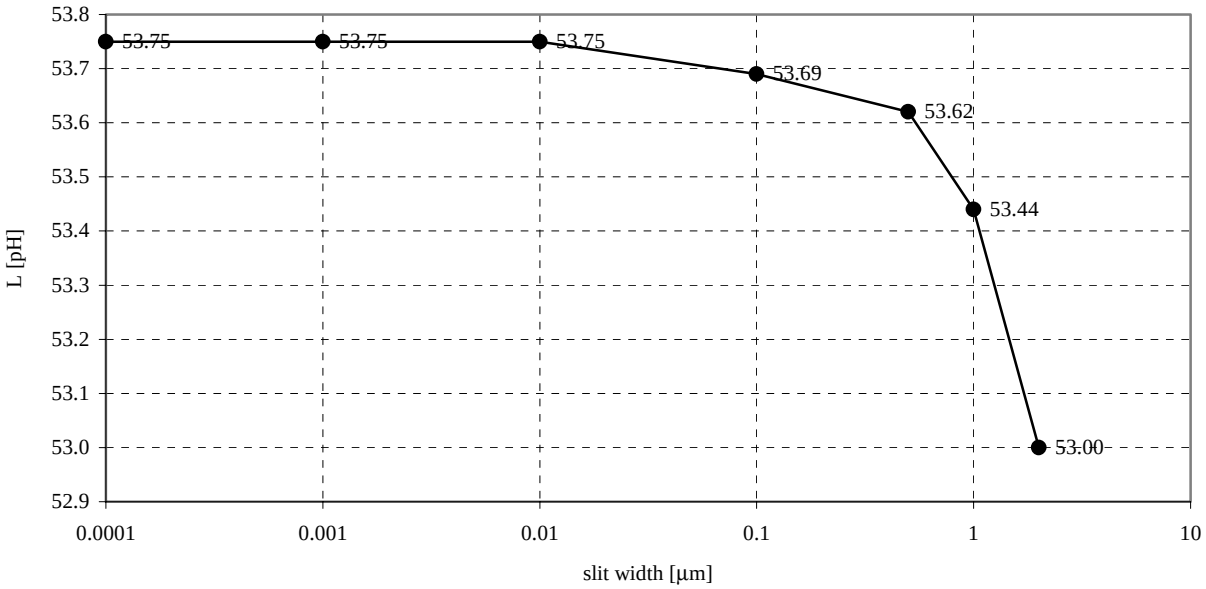

Figure 4.12: self-inductance of slitted square washer as a function of slit width.

The graph shows that as the slit narrows, the self-inductance of the washer approaches a constant value of 53.75pH, which is 0.07% lower than the result for a washer of the same dimensions but without a slit (53.79pH). This proves that for narrow slits, the approximation adopted in most works in the literature is correct.

In section 2.4, it was mentioned that the self-inductance of a square washer with a slit is generally approximated as the sum of the hole inductance and of the slit inductance [1]. This implies that the self-inductance of a square washer with a slit should be higher than that of a square washer of identical dimensions but no slit. The result from the 3D-MLSI simulations summarised in **Figure 4.12** seems to disagree with this commonly accepted assumption, but we must consider that the software calculates the self-inductance of the terminal path, which is shorter in the presence of a slit than the path followed by a current circulating around a hole. This might explain why the self-inductance is dropping as the slit width is increasing.

4.4 Kahlmann's SQUID

The final and most significant application of 3D-MLSI was the magnetometer layout considered in section 3.4 (which has been reproduced for reference in **Figure 4.13** below). Four magnetometers were considered, of expected SQUID self-inductances 50pH, 100pH, 150pH and 200pH. These values were first checked against 3D-MLSI calculations. The penetration depth was taken to be 0.23nm and the resolution step 5. Results show good agreement between the simulations and the values in [26], if the overestimation effect discussed in section 4.1 is taken into account (see **Table 4.1** below).

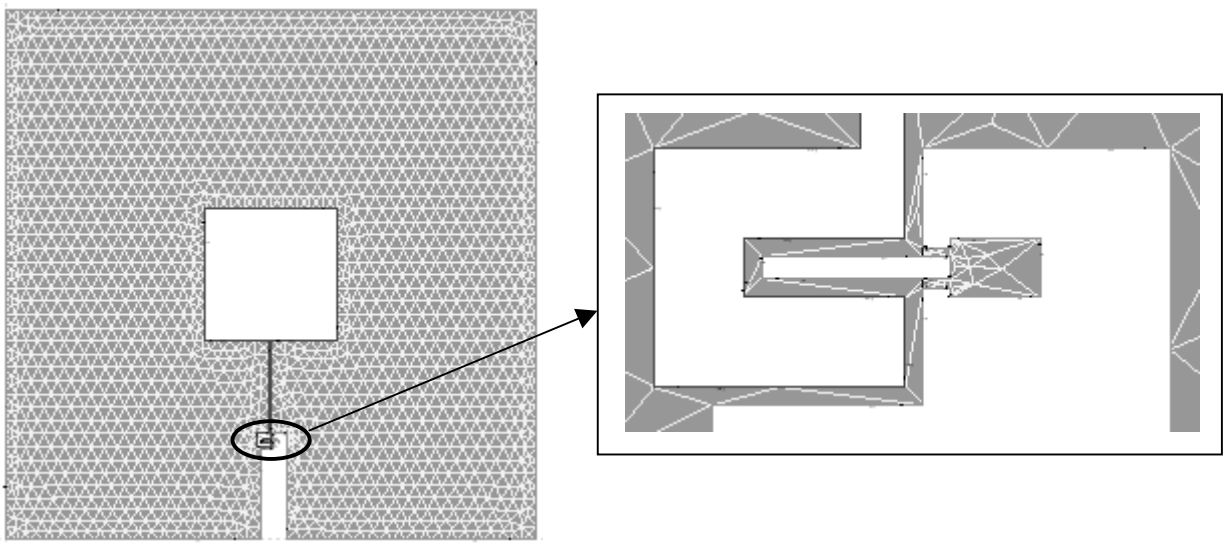

Figure 4.13: Kahlmann's SQUID layout, with the pickup loop on the left and a blow-up of the SQUID on the right.

Kahlmann et al [pH]	3D-MLSI [pH]
50	57
100	106
150	154
200	203

Table 4.1: comparison between the expected SQUID self-inductances and the values obtained by 3D-MLSI.

Using the method described in section 3.4, the equivalent mutual inductances and the effective areas of the four magnetometer layouts were calculated as a function of the distance from

the source. The aim was to verify that those parameters satisfied the properties observed for simpler superconducting systems.

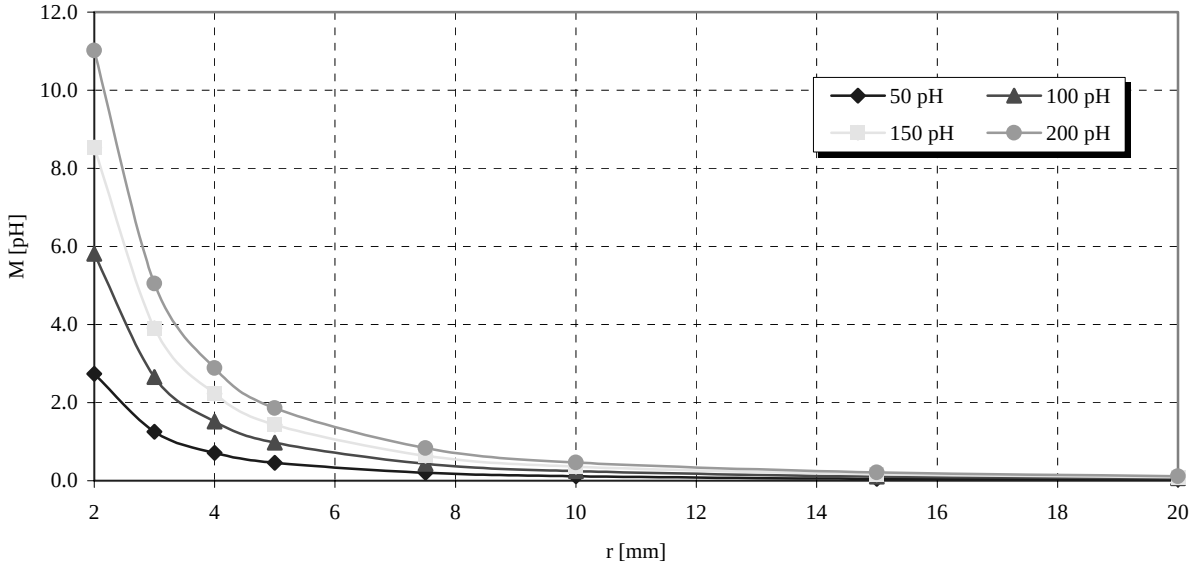

Figure 4.14: mutual inductance of the magnetometers as a function of distance from source.

Figure 4.14 shows that the mutual inductance *M* of the magnetometers approaches zero as the distance from the source increases. From previous considerations, we expect it to drop as the square of the distance. This is confirmed by the lines fitting the data points in **Figure 4.15**.

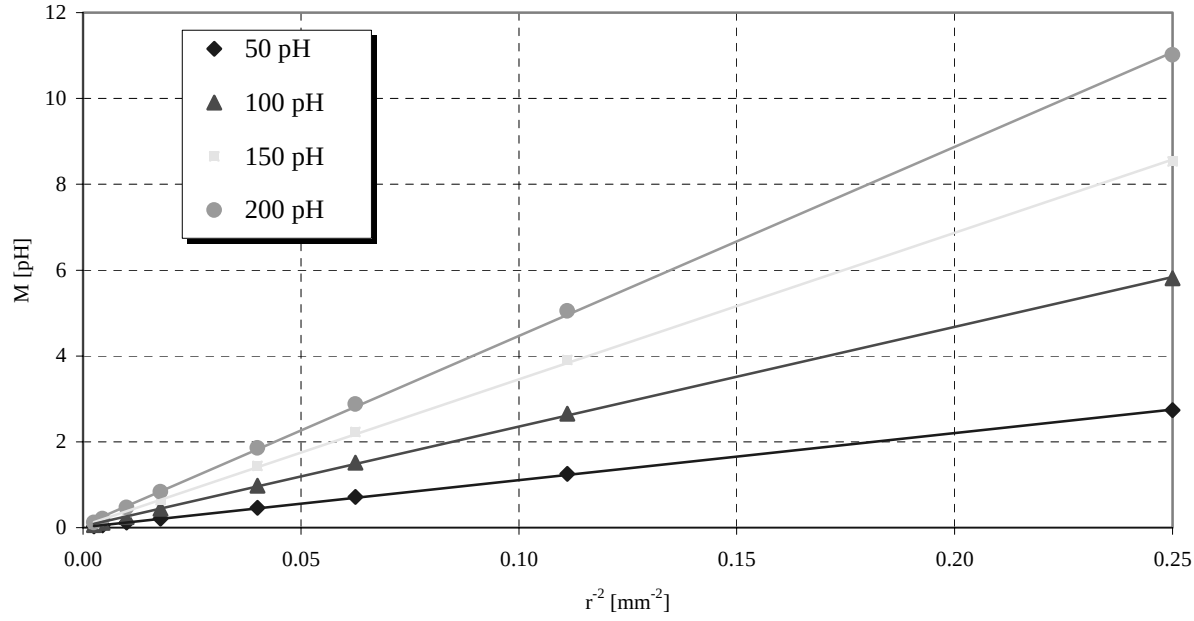

Figure 4.15: graph showing the r^{-2} dependence of the mutual inductance.

As the mutual inductance exhibits the expected dependence on the distance from the source, it follows from the definition of effective area given in section 2.3.2 that A_{eff} should approach a constant limiting value. This result has been verified in **Figure 4.16** below:

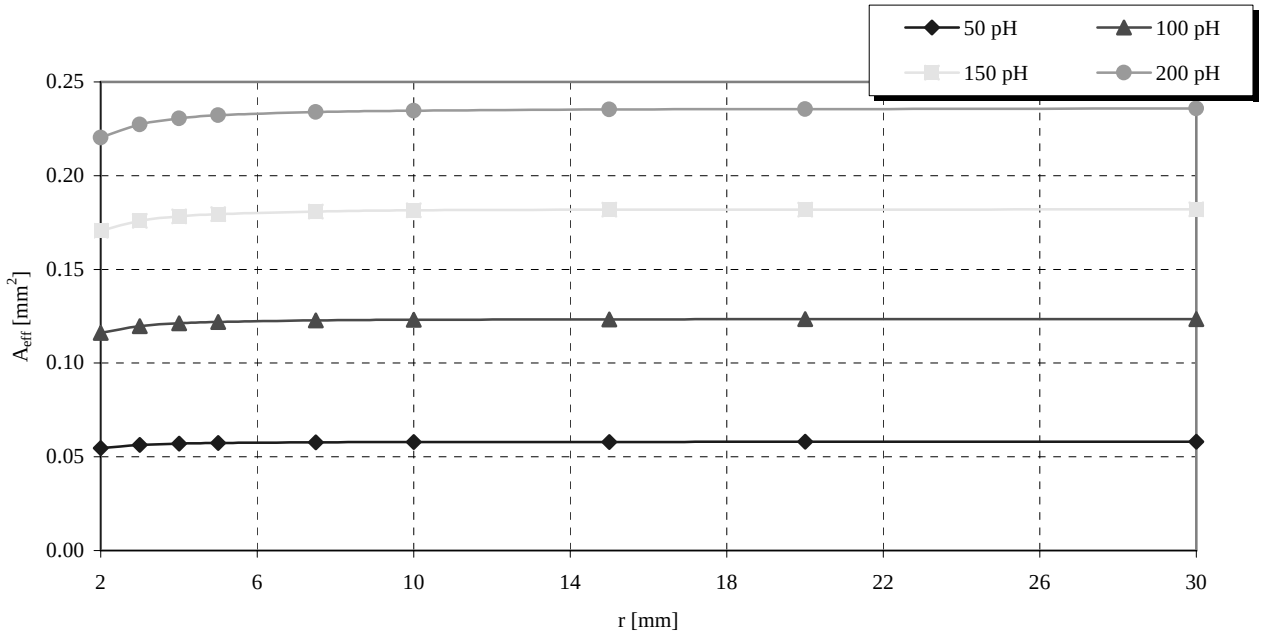

Figure 4.16: effective area as a function of distance from source. A limiting value is approached in all cases.

The most important test for the reliability of 3D-MLSI and of the technique for extraction of equivalent inductances expounded in section 3.4 is the comparison between the effective areas calculated using 3D-MLSI and the experimental results by Kahlmann et al [26]. These results are summarised in **Table 4.2** and plotted in **Figure 4.17**. In [26], the measured quantities were checked against the theoretical predictions from the formula discussed in section 2.3.2:

$$A_{eff} = \frac{L_S}{L_p} A_p + A_S \tag{2.20}$$

where L_S is the SQUID inductance, $L_p = 1.25\mu_0 d$ and $A_p = dD$ the pickup loop inductance and effective area, and A_S the SQUID effective area. A_S is usually neglected because is very small [1].

L_{SQUID}	Theoretical	Experimental	3D-MLSI
50	0.064	0.053	0.058
100	0.127	0.123	0.124
150	0.191	0.172	0.182
200	0.255	0.231	0.236

Table 4.2: comparison between the expected SQUID effective areas and the values obtained by 3D-MLSI (in mm^2).

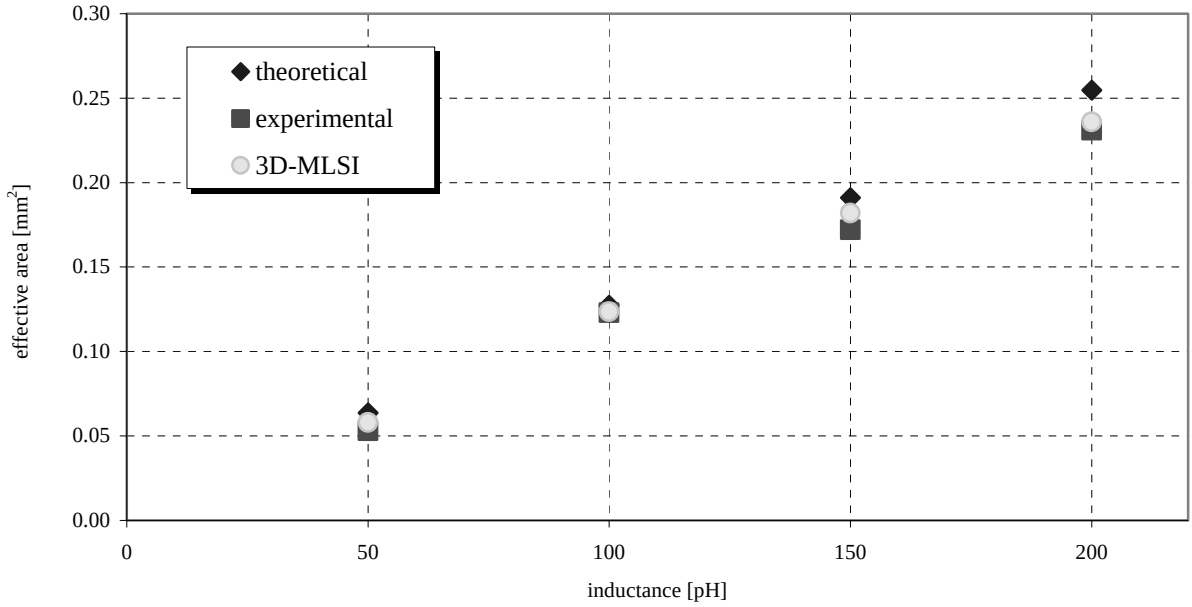

Figure 4.17: comparison between 3D-MLSI values, theoretical predictions and experimental results by Kahlmann et al.

The agreement between the 3D-MLSI results and both the theoretical predictions and experimental data is satisfactory. Not only does the program give the right value of the SQUID self-inductance, as previously shown in **Table 4.1**, but it can also produce an accurate estimate of the equivalent mutual inductance of the whole system and thus its effective area. This is evidence that the inductance matrix of 3D-MLSI is a reliable output and can be safely used to predict the parameters of real SQUID magnetometers. The fact that the 3D-MLSI values are approximately midway between the theoretical predictions and Kahlmann's experimental data is a significant indication of the important role that computational methods can play in the design of efficient superconducting sensors.

Conclusions

The aim of this project was to investigate the accuracy and flexibility of the finite element package 3D-MLSI for modelling superconducting thin film structures. Overall it was found that the computer program gives results that compare well with analytical formulae and experimental data. The accuracy of the 3D-MLSI calculations could be adjusted to obtained the desired uncertainty, showing that a trade-off between high resolution and high CPU time and memory usage can be easily attained.

The validity and accuracy of 3D-MLSI have been tested extensively, using common superconducting systems of known parameters. The precision of the calculated inductances depends on the resolution step chosen for a particular simulation. The self-inductance of a stripline proved to be consistent with theoretical predictions of both the kinetic and the magnetic inductance, showing a square dependence on the penetration depth.

The agreement between the self-inductance value for square washers found by Jaycox and Ketchen [10] and the 3D-MLSI calculations was significant for large washers with large loop-width-to-hole-width ratio, while a predicted large discrepancy was observed otherwise. The effective area of a square washer calculated with 3D-MLSI was successfully compared to the value predicted by Ketchen et al [6]. The self-inductance of the washer exhibited the same dependence on the square of the penetration depth as the stripline, while the mutual inductance was observed to reach a constant value as the current distribution on the washer becomes uniform.

The comparison between a square washer with a slit and a washer without a slit led to the conclusion that the self-inductance of the washer with a slit approaches the inductance value of the washer without a slit from below, as the slit width goes to zero.

Finally, the SQUID magnetometer layout by Kahlmann et al [26] was considered. The parameters of both a single component (the SQUID loop) and of the whole system proved consistent with Kahlmann's findings and with theoretical predictions. This result was particularly encouraging, as it proved the solid correlation between a numerical technique and experimental reality for a complex device of technological interest.

In conclusion, this project was successful in showing that 3D-MLSI can be used to predict the inductances and effective areas of real magnetometers, with good accuracy and reliability. A promising field of application for the software is design optimisation, where a good *a priori* knowledge of the main system parameters and their dependence on geometry is a great advantage for the development and fabrication of efficient devices. It would also be of scientific interest to

perform simulations on systems where no analytical results exit, but for which experimental results are easy to obtain. A direction for future work that could lead to significant applications is the study of slotted SQUIDs [27],[28], which have been claimed to greatly enhance the effective area leaving the SQUID self-inductance unchanged. Because of its great practical interest and its dependence essentially on geometry, the slotted SQUID seems to suit 3D-MLSI characteristics perfectly.

References

[1] Koelle D., Kleiner R., Ludwig F., Dantsker E. and Clarke J., *Rev. Mod. Phys.*, 1999 **71** (3) 631-686

[2] Feynman R. P., Leighton R. B. and Sands M., *The Feynman Lectures on Physics*, Reading, MA: Addison-Wesley, 1965, vol. III, section 21

[3] Waldram J. R., *Superconductivity of Metals and Cuprates*, Bristol: IOP Publishing, 1996

[4] Van Duzer T. and Turner C. W., *Principles of Superconductive Devices and Circuits*, New York: Elsevier North Holland, 1981

[5] Schrieffer J. R. and Tinkham M., *Rev. Mod. Phys.*, 1999 **71** (2) 313-317

[6] Ketchen M. B., Gallagher W. J., Kleinsasser A. W., Murphy S. and Clem J. R., *SQUID '85 – Superconducting Quantum Interference Devices and their Applications*, Berlin: de Gruyter, 1985, pp 865-871

[7] Koelle D., Miklich A. H., Ludwig F., Dantsker E., Nemeth D. T. and Clarke J., *Appl. Phys. Lett.*, 1993 **63** (16) 2271-2273

[8] Ketchen M. B., *IEEE Trans. Mag.*, 1987 **MAG-23** (2) 1650-1657

[9] Koch R. H., Umbach C. P., Clark G. J., Chaudhari P. and Laibowitz R. B., *Appl. Phys. Lett.*, 1987 **51** (3) 200-202

[10] Jaycox J. M. and Ketchen M. B., *IEEE Trans. Mag.*, 1981 **MAG-17** (1) 400-403

[11] Chang W. H., *IEEE Trans. Mag.*, 1981 **MAG-17** (1) 764-766

[12] Hildebrandt G. and Uhlmann F. H., *IEEE Trans. on Appl. Supercond.*, 1995 **5** (2) 2766-2769

[13] Khapaev M. M. Jr., *Supercond. Sci. Technol.*, 1997 **10** 389-394

[14] Lorrain P., Corson D. R. and Lorrain F., *Electromagnetic Fields and Waves*, New York: W. H. Freeman & Co, 1988

[15] Khapaev M. M. Jr., *IEEE Trans. Microwave Theory and Techn.*, 2001 **49** (1) 217-220

[16] Khapaev M. M. Jr., Kidiyarova-Shevchenko A. Y., Magnelind P. and Kupriyanov M. Y., *IEEE Trans. on Appl. Supercond*., 2001 **11** (1) 1090-1093

[17] Khapaev M. M. Jr., Kupriyanov M. Y., Goldobin E. and Siegel M., *Supercond. Sci. Technol.*, 2003 **16** (1) 24-27

[18] Khapaev M. M. Jr., *Supercond. Sci. Technol.*, 1996 **9** 729-733

[19] Silvester P. P. and Ferrari R. L., *Finite Elements for Electrical Engineers*, Cambridge University Press, 1983

[20] Khapaev M. M. Jr. and Goldobin E., *3D-MLSI: Extraction of Inductances of Multilayer Superconductor Circuits*, User's Manual, http://bmik.ru/vm/sotr/vmhap/ml/ml.html

[21] Grover F. W., *Inductance Calculation – Working Formulas and Tables*, New York: Dover Publications, 1946

[22] Tarte E.J., McBrien P.F., Ransley J.H.T., Hadfield R.H., Inglessi E., Booij W.E., Burnell G., Blamire M.G. and Evetts J.E., *IEEE Trans. Appl. Supercond.*, 2001 **11** (1) 418-421

[23] Rose-Innes A. C. and Rhoderick E. H., *Introduction to Superconductivity*, Oxford: Pergamon Press, 1978, p. 21

[24] Lee L. P., Longo J., Vinetskiy V. and Cantor R., *Appl. Phys. Lett.*, 1995 **66** 1539-1541

[25] Cantor R., Lee L. P., Teepe M., Vinetskiy V. and Longo J., *IEEE Trans. Appl. Supercond.*, 1995 **5** 2927-2930

[26] Kahlmann F., Booij W. E., Blamire M. G., McBrien P. F., Peng N. H., Jeynes C. and Tarte E. J., *Appl. Phys. Lett.*, 2000 **77** 567-569

[27] Jansman et al, *Appl. Phys. Lett.*, 1998 **72** 3515

[28] Jansman et al, *IEEE Trans. Appl. Supercond.*, 1999 **9** 3290